4/p

N63-14589

Code-1

TECHNICAL NOTE

D-1779

LOW-SPEED WIND-TUNNEL INVESTIGATION OF AN ANNULAR-JET

CONFIGURATION IN GROUND PROXIMITY

By James H. Otis, Jr., and Kenneth W. Goodson

Langley Research Center
Langley Station, Hampton, Va.

NATIONAL AERONAUTICS AND SPACE ADMINISTRATION

WASHINGTON   April 1963

5-54163

52p

NATIONAL AERONAUTICS AND SPACE ADMINISTRATION

TECHNICAL NOTE D-1779

LOW-SPEED WIND-TUNNEL INVESTIGATION OF AN ANNULAR-JET

CONFIGURATION IN GROUND PROXIMITY

By James H. Otis, Jr., and Kenneth W. Goodson

SUMMARY

An investigation to determine the ground-effect characteristics of a
42-inch-diameter annular-jet model, at forward speeds up to 100 feet per second,
has been conducted in the 17-foot test section of the Langley 300-MPH 7- by
10-foot tunnel.

The results of the investigation indicated that at zero angle of attack a
rapid increase in lift augmentation was obtained with forward speed and this
variation was relatively independent of the height-diameter ratio. Relatively
large drag forces, of which the inlet momentum drag was a predominant factor,
were measured at the higher velocity ratios. At the low height-diameter ratios
and low velocity ratios, however, the total measured drag was less than the cal-
culated inlet momentum drag. At the low velocity ratios the rate of increase of
the pitching-moment parameter with respect to velocity ratio decreased as the
ground was approached.

INTRODUCTION

A considerable amount of both theoretical and experimental research has
been done on the lift-augmentation characteristics of annular-jet ground-effect
machines in hovering. Some work, although not as extensive as that done at zero
speed, has been done on the forward-speed characteristics. (See refs. 1, 2,
and 3.)

The present model was constructed to obtain some information on the wave-
drag characteristics of an annular-jet configuration in over-water operation.
Some of the results obtained in a hydrodynamic towing tank at Langley Research
center over water and over a ground board at forward speeds are presented in
reference 1. The model was also tested in the 17-foot test section of the
Langley 300-MPH 7- by 10-foot tunnel. Some of these results are also presented
in reference 1 to show the effects of ground-board boundary layer. The effects
of ground height and angle of attack were not available at the time reference 1
was presented and are presented herein.

The positive senses of forces, moments, and angles are indicated in figure 1.

D   drag, lb

d   vehicle nozzle diameter, 3.50 ft

h   height above ground plane (measured at center of model), ft

L   lift, lb

M   pitching moment, ft-lb

m_j mass rate of jet airflow, slugs/sec

N   propeller rotational speed, rpm

p_b base-plate pressure measured with respect to free-stream static pressure, lb/sq ft

p_∞ free-stream static pressure, lb/sq ft

Δp_b average increment of base-plate pressure, $p_b - p_\infty$, lb/sq ft

p_t total pressure measured with respect to free-stream static pressure, lb/sq ft

Δp_t average increment of jet total pressure, $p_t - p_\infty$, lb/sq ft

V_j average exit velocity of annular jet, ft/sec

V_∞ free-stream velocity, ft/sec

α angle of attack of base plate with respect to ground plane, deg

$\dfrac{D}{m_j V_j}$ nondimensional drag parameter

h/d   ratio of height above ground plane to nozzle diameter

$\dfrac{L}{m_j V_j}$ nondimensional lift parameter

$\dfrac{M}{Ld}$ nondimensional pitching-moment parameter

2

$\dfrac{V_\infty}{V_j}$ ratio of free-stream velocity to average jet-exit velocity

R   Reynolds number based on nozzle diameter

MODEL AND APPARATUS

A photograph of the model and ground-board installation in the 17-foot test section of the Langley 300-MPH 7- by 10-foot tunnel is presented in figure 2(a) and shows the general test arrangement. Figure 2(b) shows the details of the model which consisted of a 42-inch circular plenum chamber with a ratio of depth to diameter of 0.143. A 15-inch ducted propeller driven by a 10-horsepower three-phase induction motor was mounted with the thrust axis perpendicular to the top surface of the plenum chamber. A base plate 39 inches in diameter was attached to the plenum chamber with eight equally spaced 3/4-inch-diameter support members. The annular-jet vehicle has a jet area of 1.33 square feet and a total planform area (based on d) of 9.62 square feet, which results in a ratio of jet area to total planform area of 13.8 percent.

Eleven static-pressure orifices were located on the base semispan along radial lines from the center (fig. 2(b)) in order to obtain the base pressures. Total-pressure rakes spanned the jet exit at eight stations around the annulus at 45° intervals. These four-tube rakes were manifolded and read as an average total pressure at each station.

No attempt was made to obtain good internal-flow characteristics, and the flow was allowed to seek the path of least resistance. Because of the manner of base-plate attachment the velocity distribution was not as uniform as desired.

A three-component strain-gage balance was used to measure lift, drag, and pitching moment. This balance was attached to a single-strut support system with provisions for changing the model attitude and height with respect to the ground plane. The balance was attached to the model well above the top of the inlet duct. (See fig. 2(b).)

TESTS AND METHODS

The investigation was conducted in the 17-foot test section of the Langley 300-MPH 7- by 10-foot tunnel. The effects of the ratio of height above ground to diameter of vehicle nozzle, as a function of velocity ratio, were investigated with the model at zero angle of attack. For these tests the height-diameter ratio varied from 0.02 to 1.27. Angle-of-attack effects as a function of velocity ratio were investigated at height-diameter ratios of 0.05 and 0.10. At h/d = 0.05, the angles of attack investigated were 0°, ±1°, and ±2°; at h/d = 0.10, the angles of attack investigated were 0°, ±2°, ±5°, and ±8°. The angle of attack for a given ground height was limited by model contact with the ground.

In order to evaluate the data, the characteristics of the flow around and emitting from the model had to be determined. Static pressures were measured on the base as indicated in figure 2(b), and total jet-exit pressures were determined as discussed in the section entitled "Model and Apparatus." The base pressures and the jet total pressures were averaged over the base and around the jet annulus, respectively. The jet-exit static pressures were determined by assuming that the static pressure varied linearly from the base-pressure value at the inside edge of the jet to the free-stream static pressure outside the jet. From these pressure measurements the jet mass flow, jet-exit velocities, and so forth were determined.

The data were obtained at two propeller rotational speeds through a range of free-stream velocities from 0 to 100 feet per second in order to obtain overlapping data covering the velocity-ratio range from 0 to about 2.1. The Reynolds number range, based on the model nozzle diameter, is presented in figure 3 as a function of velocity ratio for the two rotational speeds investigated. The pitching-moment data were transferred from the balance center of gravity to a point 10 percent of the vehicle diameter above the base plate.

<div align="center">PRESENTATION OF RESULTS</div>

The results of the investigation are presented in the following figures:

<div align="center">RESULTS AND DISCUSSION</div>

<div align="center">Basic Data</div>

The basic data of this investigation are presented in figures 4 to 6. The lift and drag data are nondimensionalized by dividing by $m_j V_j$ and are presented as a function of the ratio of the free-stream velocity to the average jet-exit velocity V_∞/V_j for two propeller rotational speeds N. This method of correlating the nondimensional data practically eliminates the effects of N because the force and moment coefficients and the velocity ratios are both functions of N. The pitching-moment data were nondimensionalized by dividing by the product

of the lift and nozzle diameter Ld. Also presented as a function of velocity ratio are the parameters necessary to obtain a complete set of dimensional data, namely, the mass rate of airflow through the system, the average jet-exit velocity, the average total-pressure increment in the annular jet, and the average base-pressure increment.

The basic data are organized in three distinct groups. Figure 4 presents the effects of height-diameter ratio with the model at zero angle of attack. Figures 5 and 6 present the effects of angle of attack at height-diameter ratios of 0.05 and 0.10, respectively. In these tests the rotational speed of the ducted propeller was held constant through the height and the free-stream-velocity ranges. As a result of holding the rotational speed constant, the increment of total pressure in the jet and the average jet-exit velocity increase as the ground plane is approached under static conditions $\left(V_\infty/V_j = 0\right)$.

An examination of the base-pressure increment at zero angle of attack (fig. 4) shows that no appreciable base lift is obtained until the model approaches a height-diameter ratio of approximately 0.20. Even at this value of h/d positive base lift only occurs at the low velocity ratios. With further decrease in h/d, the base pressure increases rapidly and is reflected in the large gains in lift augmentation at a velocity ratio of zero. At the low height-diameter ratios, the base pressure decreased considerably at the high values of velocity ratio beginning at a value of V_∞/V_j of about 0.6 or 0.8. (See figs. 4(f) and 4(g).) This result is due to drop off of the average jet-total-pressure increment with forward speed at low height-diameter ratios. It should be noted that the ratio of the base-pressure increment to the total-jet-pressure increment at low values of h/d is approximately constant for the range of velocity ratios investigated.

Figures 5 and 6 indicate an angle-of-attack effect on the base-pressure increment at positive angles of attack. This result is due to the fact that the rear lip of the vehicle moves closer to the ground plane with increasing angle of attack and an appreciable ram effect is created.

Lift Characteristics

The lift augmentation at zero speed is dependent upon the pressures acting on the base of the model. However, at forward speed the overall lift becomes significantly larger at velocity ratios greater than about 0.6. (See fig. 7.) From the previous discussion in the section entitled "Basic Data," the base pressure (base lift) decreases at low height-diameter ratios at velocity ratios above 0.6. (See figs. 4 to 6.) This result indicates that the increase in lift is of an aerodynamic nature since the base lift is being reduced. Figure 7 shows that the increase in lift with velocity ratio is approximately the same at all ground heights for $\alpha = 0^\circ$. Further increase in aerodynamic lift is obtained with positive increase in angle of attack (figs. 8 and 9, at high velocity ratios) as a result of an increase in ram beneath the surface when in ground effect. (See refs. 4 and 5.) At low velocity ratios and low values of h/d, the effects of angle of attack are varied, probably as a result of more pronounced effects of base pressure and jet effects.

Drag Characteristics

A summary of the nondimensional drag data is presented in figures 10 to 12 to indicate the effects of velocity ratio, ground proximity, and angle of attack.

Effect of ground proximity.- Any system which brings a large mass of air into a vehicle and turns it through an angle results in a large momentum drag or so-called inlet drag. If the inlet drag $m_j V_\infty$ is nondimensionalized on the basis of momentum thrust $m_j V_j$, it is seen that the resulting inlet-drag parameter is equal to the velocity ratio. The inlet drag is presented in figures 10 to 12 in this manner.

The effects of velocity ratio and height-diameter ratio on the nondimensional drag parameter are summarized in figure 10. As the vehicle approaches the ground plane a reduction of total drag occurs at the low height-diameter ratios. It is seen in figure 10 that at a height-diameter ratio of 0.02 and $\alpha = 0^\circ$, the total drag is less than the nondimensional inlet drag between a velocity ratio of 0 and 1.0. This characteristic is not evident at the large height-diameter ratios.

It should be noted that the investigation of reference 1 was performed with the same model but with a different test technique. The model was mounted beneath the carriage in a hydrodynamic towing tank at Langley Research Center and was driven through a speed range over water and a fixed ground board. The same drag reduction obtained in the towing-tank investigation was obtained in the present wind-tunnel investigation, which indicates that the drag reduction is not caused by the mixing of the jet sheet and the boundary layer on the ground plane in the tunnel tests, but rather by a jet-flap type of effect (ref. 6) in which induced thrust is obtained even with the jet sheet deflected 90° (vertical) at the exit. The effect of the inlet on the flow over the upper surface of the model and, also, possible changes in the flow angle of the jet sheet in ground proximity may contribute to the differences shown.

Effect of angle of attack.- Figures 11 and 12 compare the nondimensional drag parameter as a function of velocity ratio for various angles of attack at height-diameter ratios of 0.05 and 0.10, respectively. At zero speed and velocity ratios below about 0.6, the drag curves are displaced by an increment which is essentially a component of the resultant force at a given angle of attack. Above a velocity ratio of about 0.6 the drag varies considerably at $h/d = 0.10$ apparently because of separation effects on the upper surface and inlet lip and suction losses on the base as evidenced by the large drag values at $\alpha = \pm 8^\circ$.

Pitching-Moment Characteristics

The pitching-moment data were nondimensionalized by dividing by the product of the total lift and the model nozzle diameter so that the parameter M/Ld represents the ratio of the shift in center of total lift to the model diameter. Therefore, if $M/Ld = 0.01$, the position of the total lift force is 1 percent of the model diameter away from the moment reference center.

Figure 13 indicates that for low velocity ratios the rate of change of the pitching-moment parameter with respect to velocity ratio decreases as the ground is approached. At a given height-diameter ratio (figs. 14 and 15), angle of attack has little effect on the pitching-moment parameter except at extreme values of α.

The pitching-moment data in general are characterized by the large moment due to the inlet drag on the high inlet which causes a large nose-up moment with velocity ratio at a given value of h/d. The break in the pitching-moment curves is probably due to several factors, namely, the base-pressure distribution as a function of forward speed, duct-inlet stall, and the decay of the jet sheet on the ground plane as a function of velocity ratio and height-diameter ratio. Reference 1 indicates that there is an increase in local base pressure with forward speed predominately on the rear part of the base creating a nose-down pitching-moment increment due to base pressure. As was mentioned previously, however, there is no appreciable base-pressure increment until the model approaches a low height-diameter ratio of about 0.20, and therefore the distribution of base pressure is not a factor until this value of h/d is reached.

Another factor that may contribute to the break in the pitching-moment curves at the higher velocity ratios is the diving moment associated with a jet-flap type of flow. Photographs of tufts showing flow patterns for various velocity ratios (figs. 16 to 18) indicate the decay of the jet sheet on the upstream side of the model, and show that as the model moves away from the ground the jet sheet decays at a lower value of velocity ratio. The velocity ratio at which the jet sheet no longer flows upstream corresponds roughly to the break in the pitching-moment curves which indicates that the model is probably operating somewhat like a jet flap.

SUMMARY OF RESULTS

A low-speed wind-tunnel investigation of a 42-inch-diameter annular-jet configuration in ground proximity has indicated the following results:

1. At zero angle of attack the present model exhibited a rapid increase in lift augmentation with forward speed and this variation was relatively independent of the height-diameter ratio.

2. Low angles of attack had little effect on lift augmentation at the low velocity ratios, but aerodynamic lift was increased rapidly above a velocity ratio of about 0.6 at the higher positive angles of attack.

3. Inlet momentum drag was a large part of the relatively large drag forces measured at the higher velocity ratios. However, at the low height-diameter ratios and low velocity ratios, the total measured drag was less than the calculated inlet momentum drag.

4. Large angles of attack had considerable effect on the nondimensional drag parameter at the higher velocity ratios.

5. At low velocity ratios the rate of increase of the nondimensional pitching-moment parameter with respect to velocity ratio decreased as the ground plane was approached. The velocity ratio at which the pitching-moment parameter reached a maximum appears to coincide with the velocity ratio at which the front of the jet sheet breaks down.

Langley Research Center,
    National Aeronautics and Space Administration,
        Langley Station, Hampton, Va., January 29, 1963.

REFERENCES

1. Kuhn, Richard E., and Carter, Arthur W.: Research Related to Ground Effect Machines. Symposium on Ground Effect Phenomena, Oct. 21-23, 1959, pp. 23-43. (Sponsored by Dept. Aero. Eng., Princeton Univ. and U.S. Army TRECOM.)

2. Kuhn, Richard E., Carter, Arthur W., and Schade, Robert O.: Over-Water Aspects of Ground-Effect Vehicles. Paper No. 60-14, Inst. Aero. Sci., Jan. 1960.

3. Jones, R. Stanton: Some Design Problems of Hovercraft. Paper No. 61-45, Inst. Aerospace Sci., Jan. 1961.

4. Fink, Marvin P., and Lasfinger, James L.: Aerodynamic Characteristics of Low-Aspect-Ratio Wings in Close Proximity to the Ground. NASA TN D-926, 1961.

5. Carter, Arthur W.: Effect of Ground Proximity on the Aerodynamic Characteristics of Aspect-Ratio-1 Airfoils With and Without End Plates. NASA TN D-970, 1961.

6. Lowry, John G., Riebe, John M., and Campbell, John P.: The Jet-Augmented Flap. Preprint No. 715, S.M.F. Fund Paper, Inst. Aero. Sci., Jan. 1957.
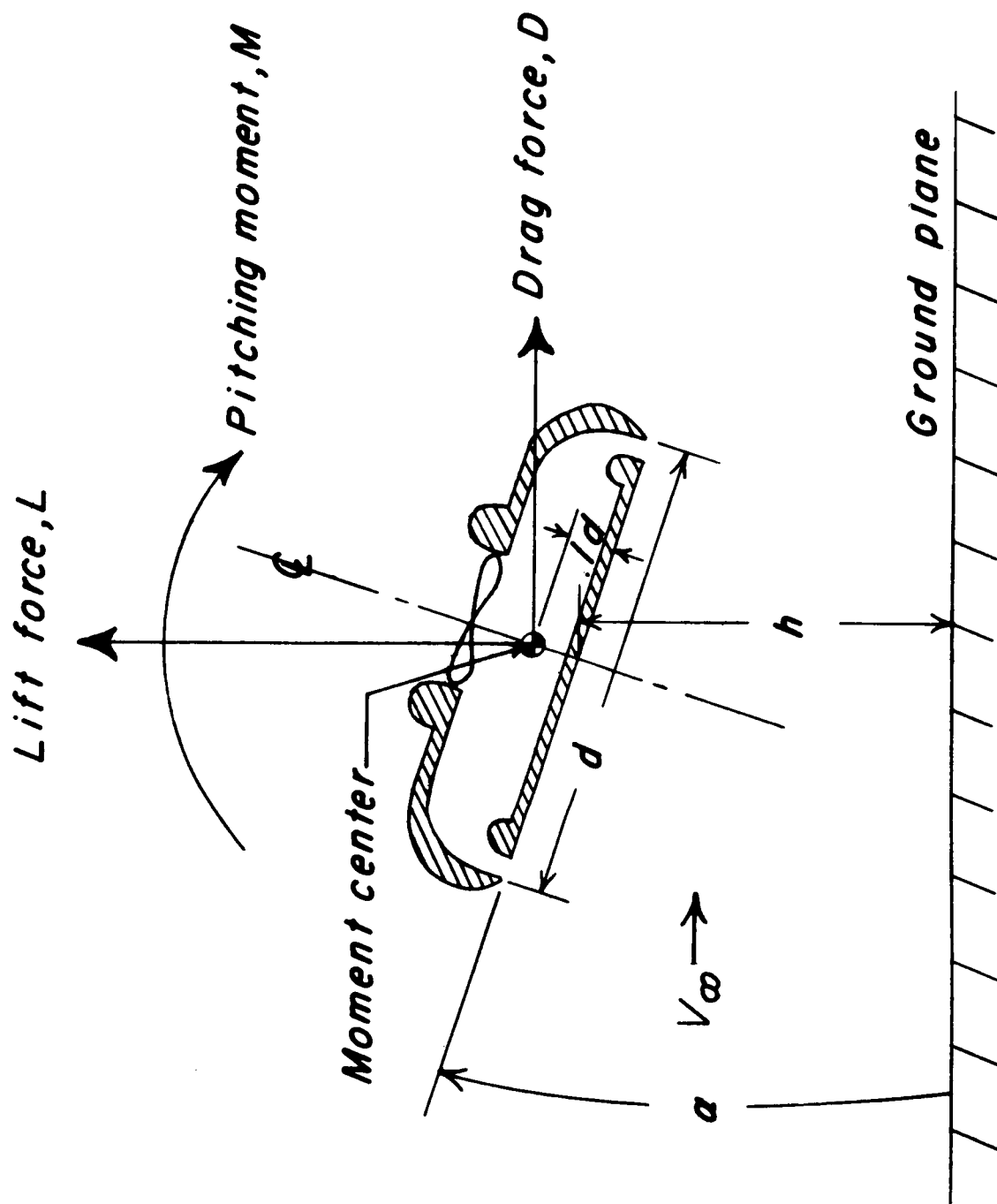
Figure 1.- Axis system showing positive forces, moments, and angles.

9
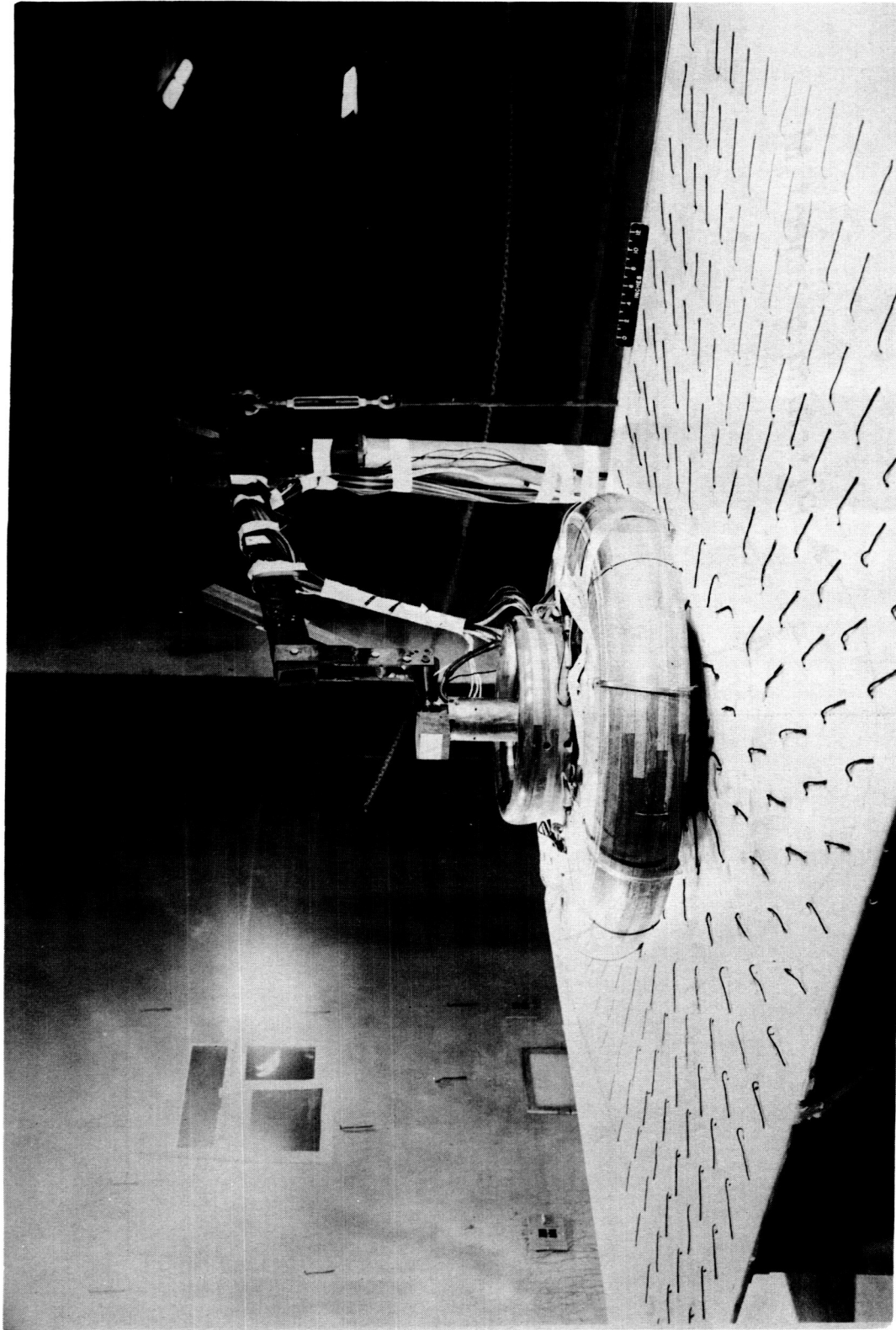
(a) Photograph of model and ground-plane installation in tunnel.

Figure 2.- Photograph and drawing of model.

L-59-5431

45°

V_∞

Propeller

11 base-plate
pressure orifices

Total-head rakes
(Eight around periphery)

8.5

17.0

A   A

Balance center of gravity

Electric motor

$19\frac{7}{8}$

r = 1

6

0.10d

Moment reference

1.5

.5

39

42

45

7

Total-head rake

Section A-A
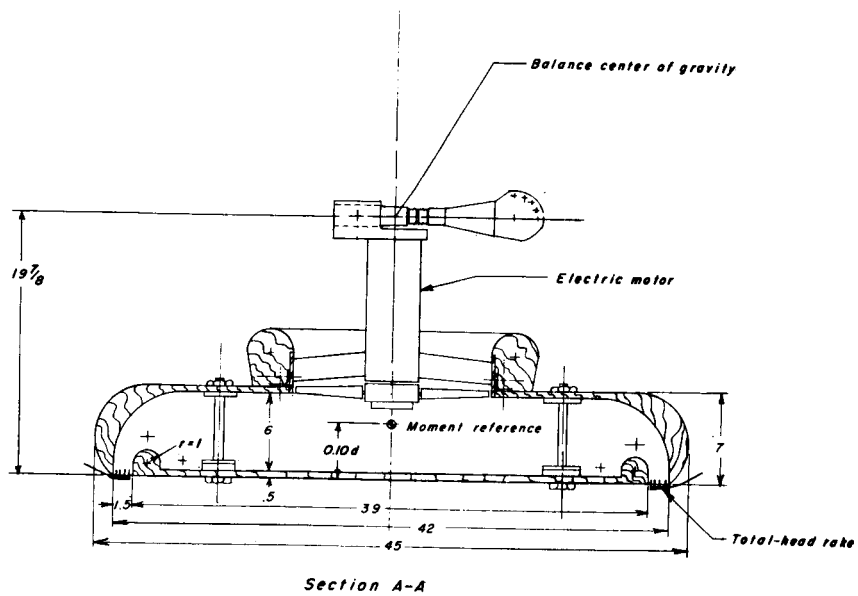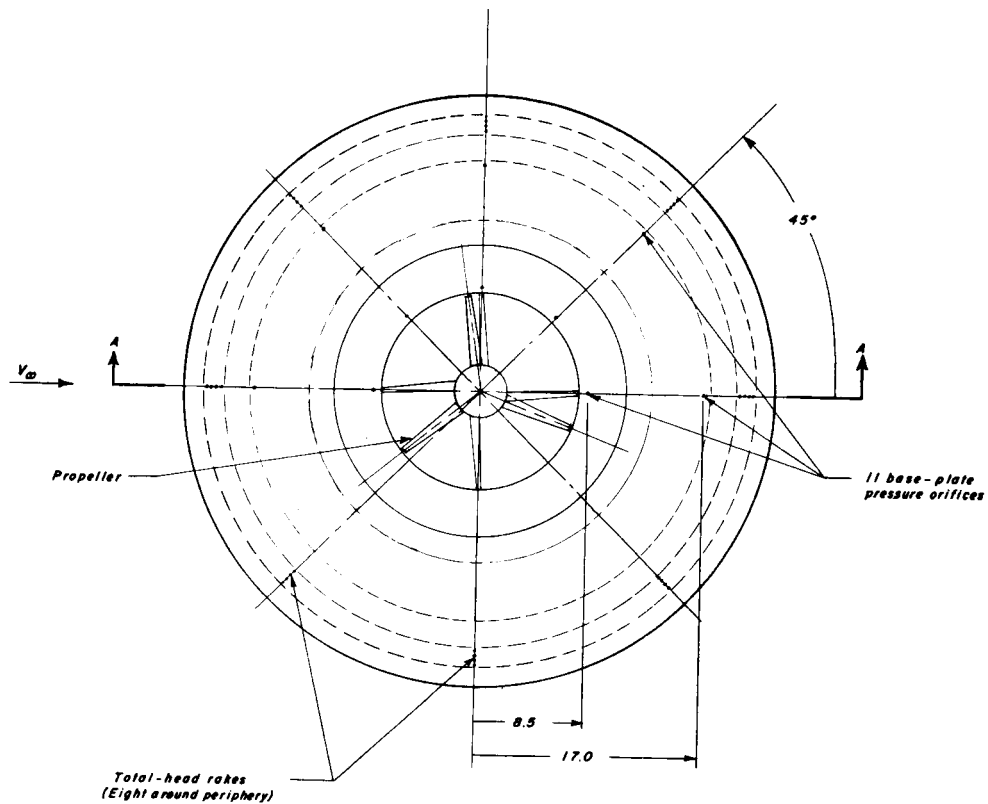
(b) Drawing of model. All dimensions are in inches unless otherwise noted.

Figure 2.- Concluded.

11
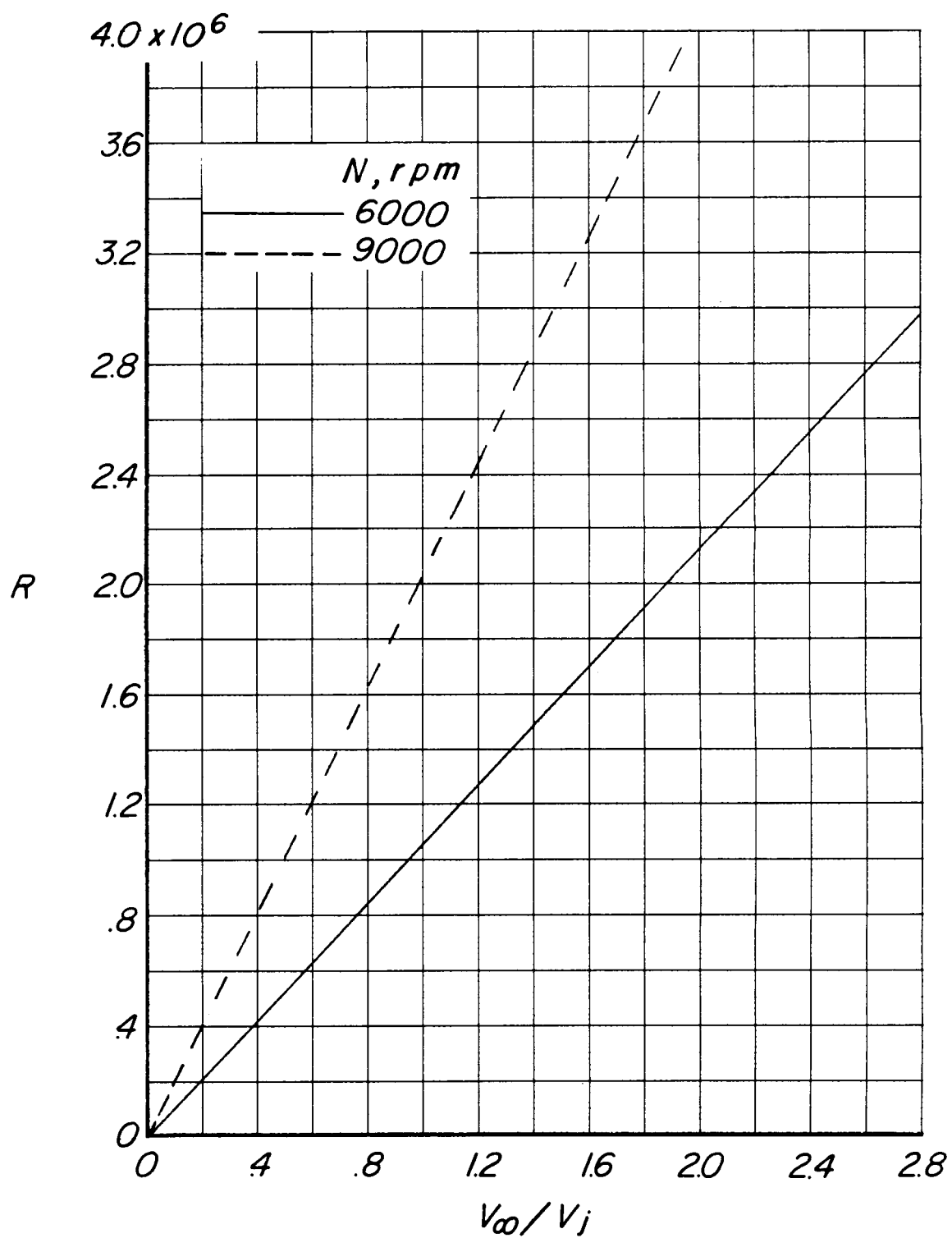
Figure 3.- Variation of Reynolds number with velocity ratio.

N, rpm
○ 6000
□ 9000
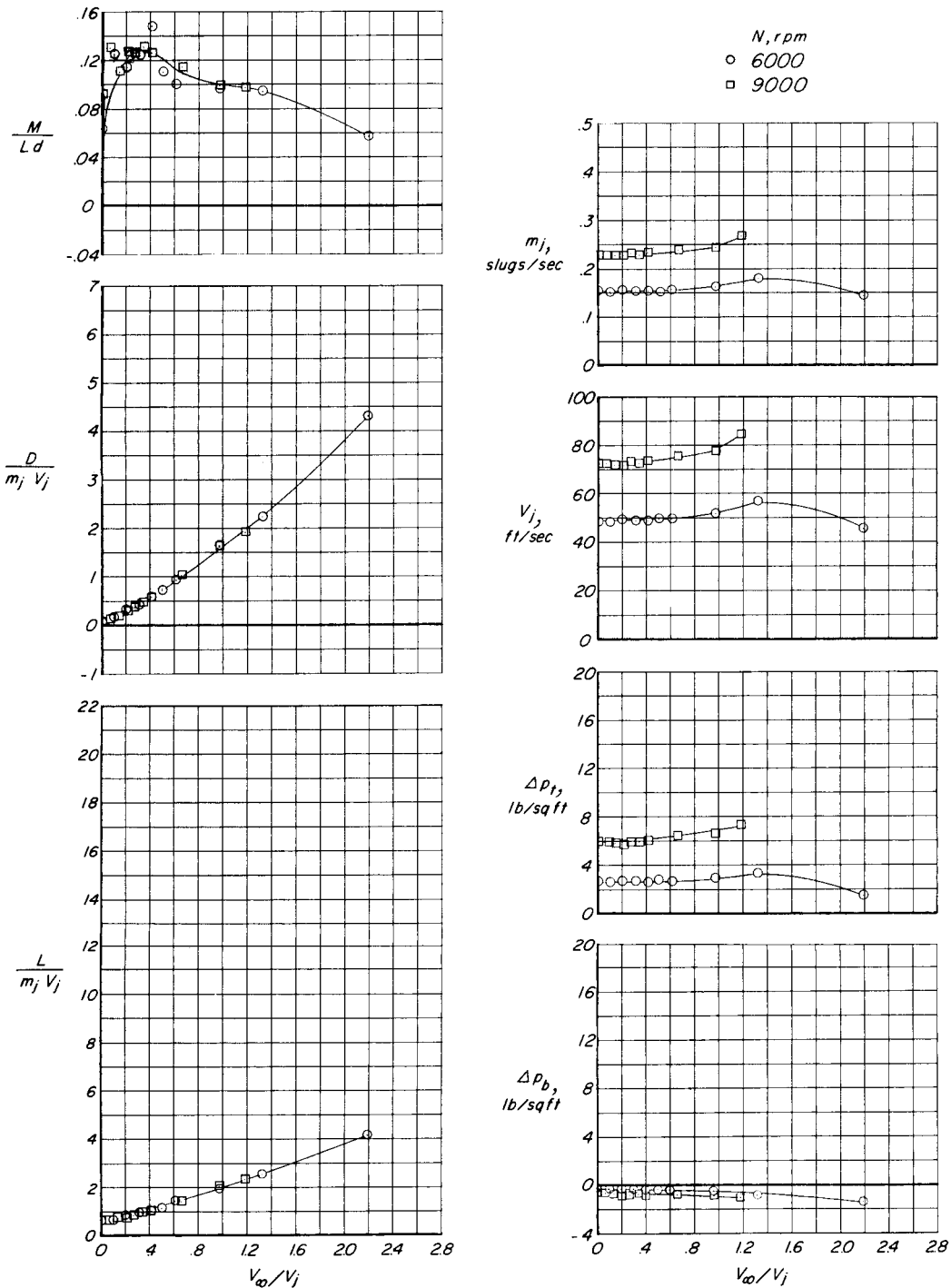
(a) h/d = 1.27.

Figure 4.- Basic data as a function of velocity ratio at zero angle of attack for a range of height-diameter ratios.
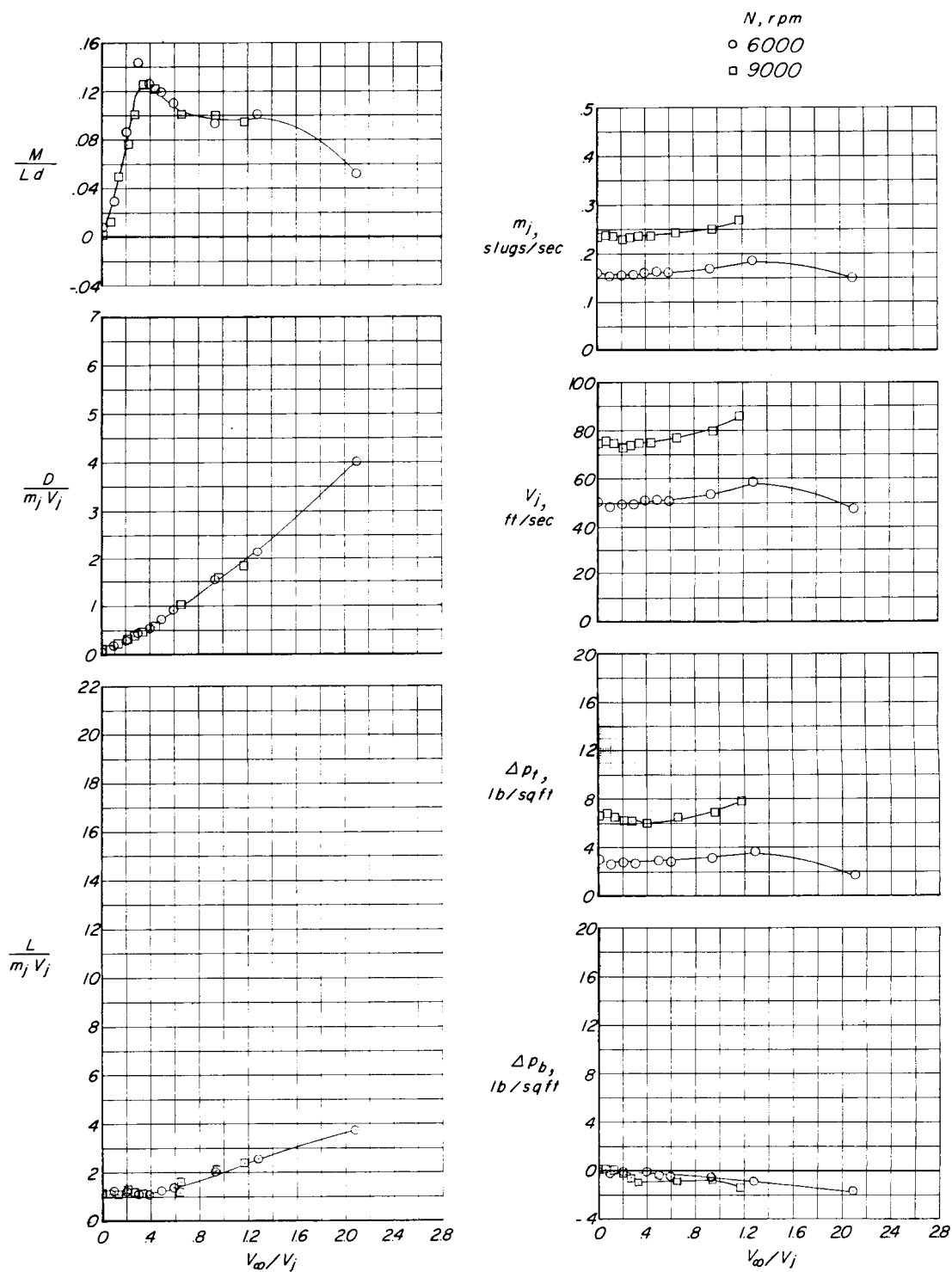
(b) h/d = 0.60.

Figure 4.- Continued.
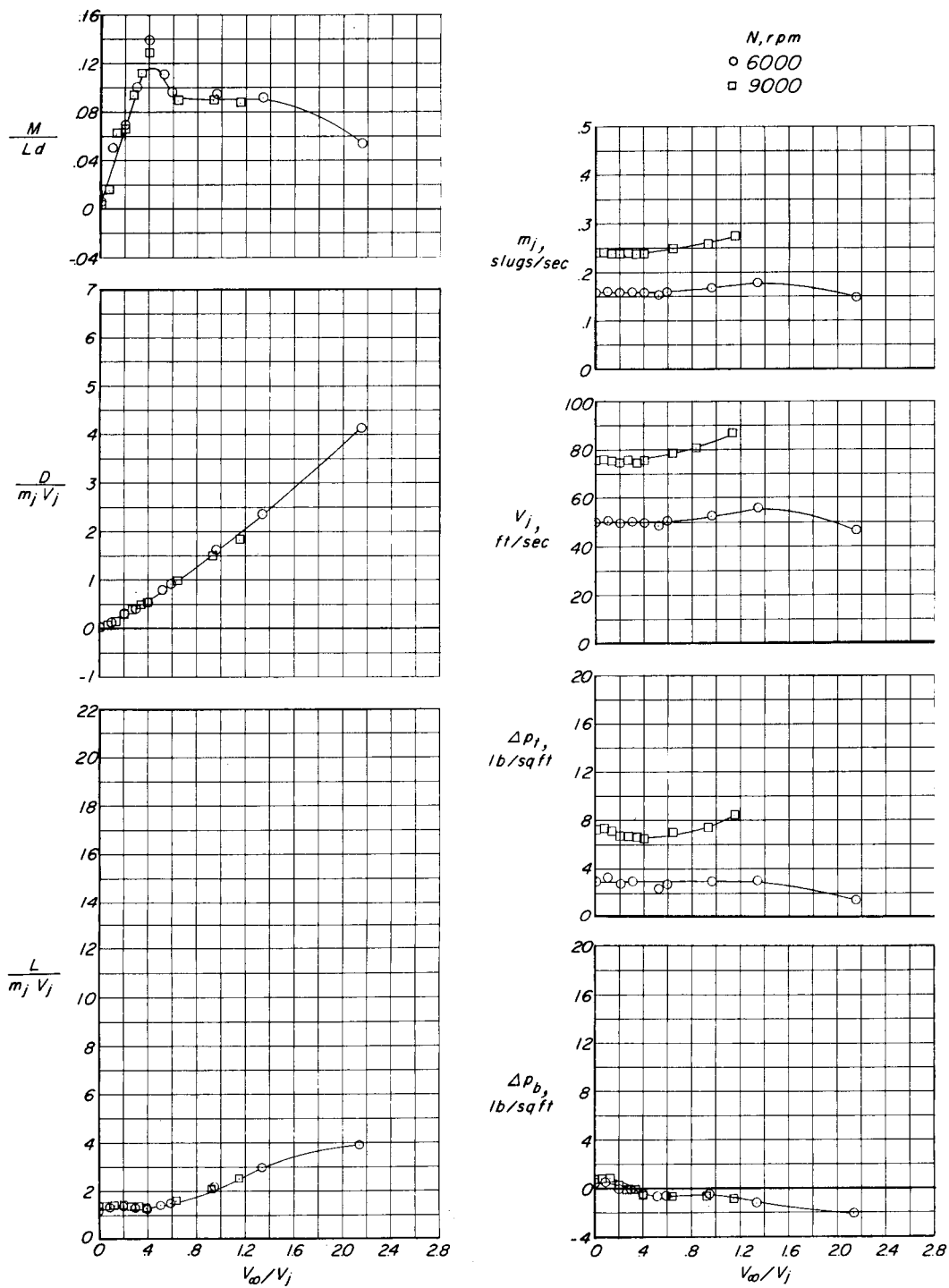
(c) h/d = 0.40.

Figure 4.- Continued.
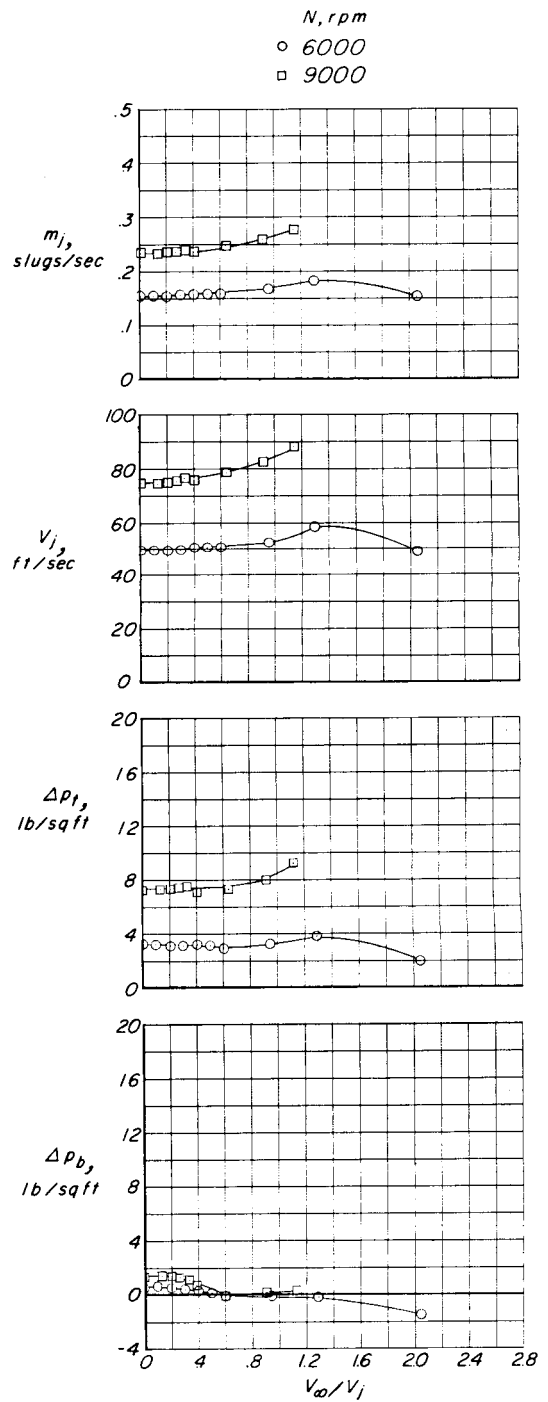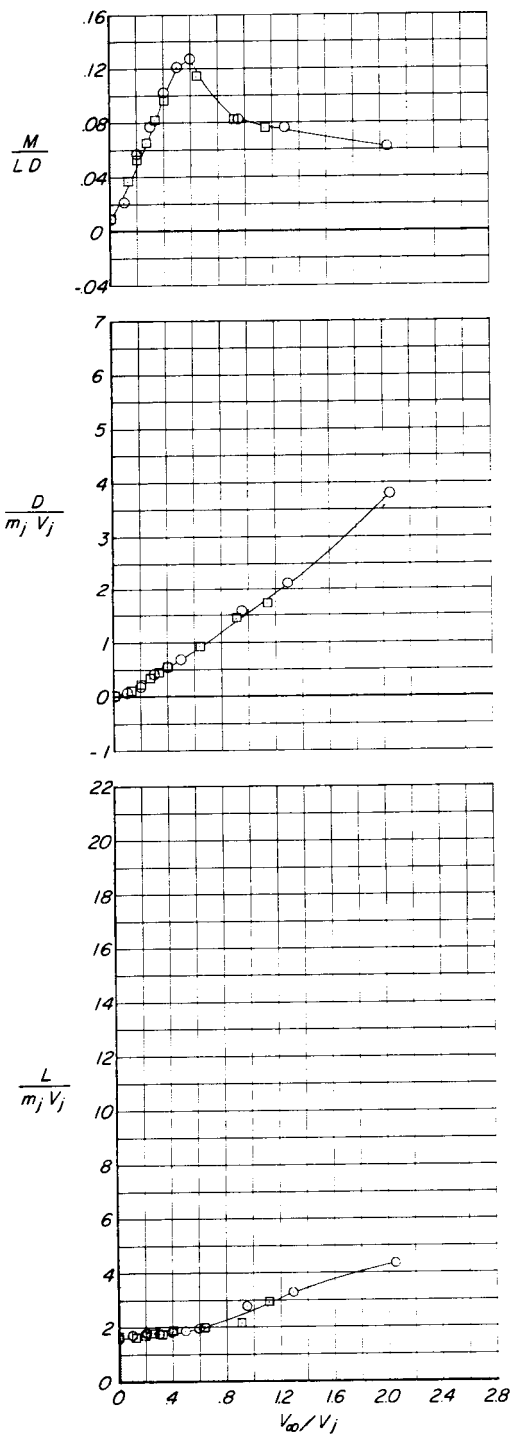
(d) h/d = 0.21.

Figure 4.- Continued.
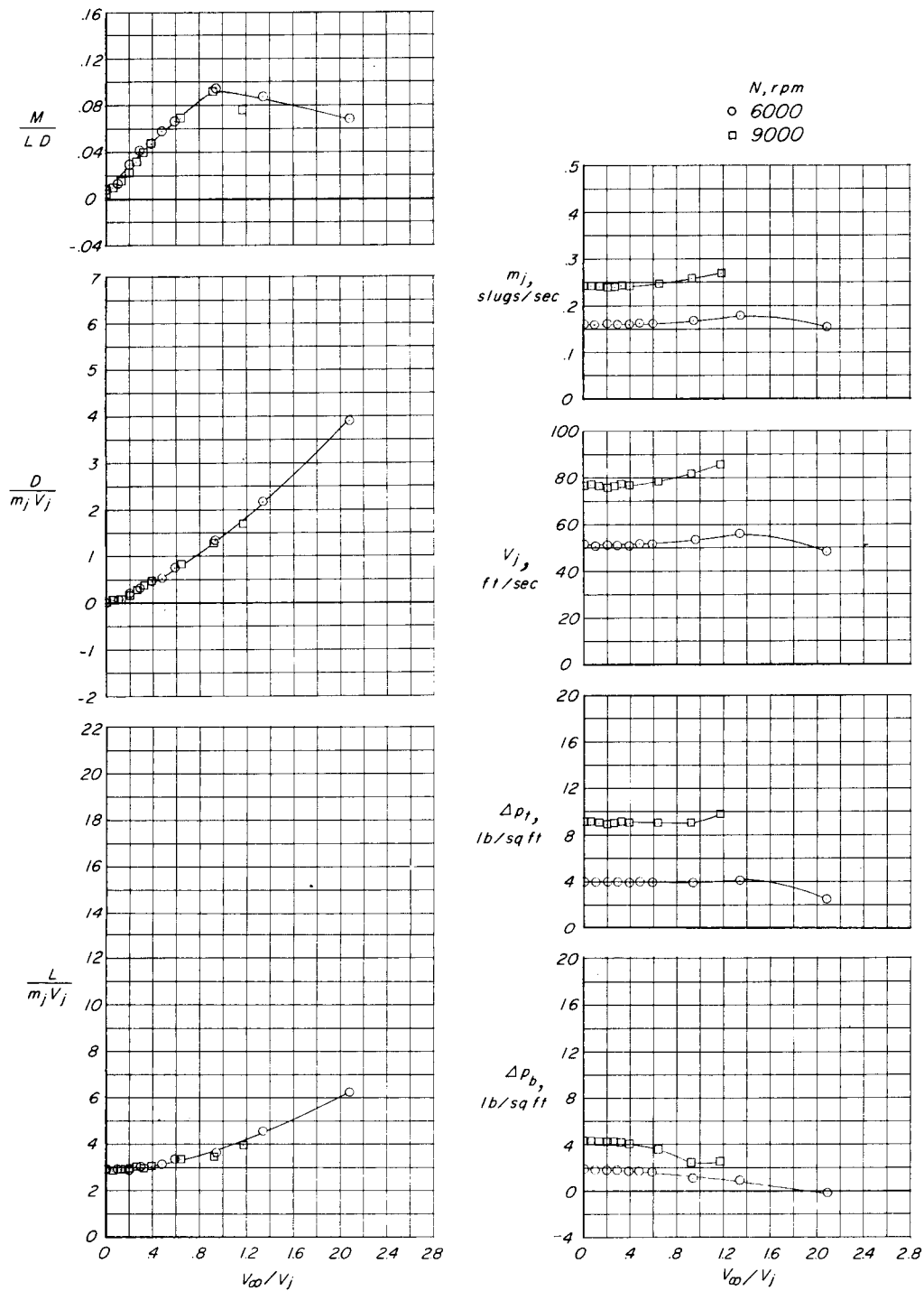
(e) h/d = 0.10.

Figure 4.- Continued.
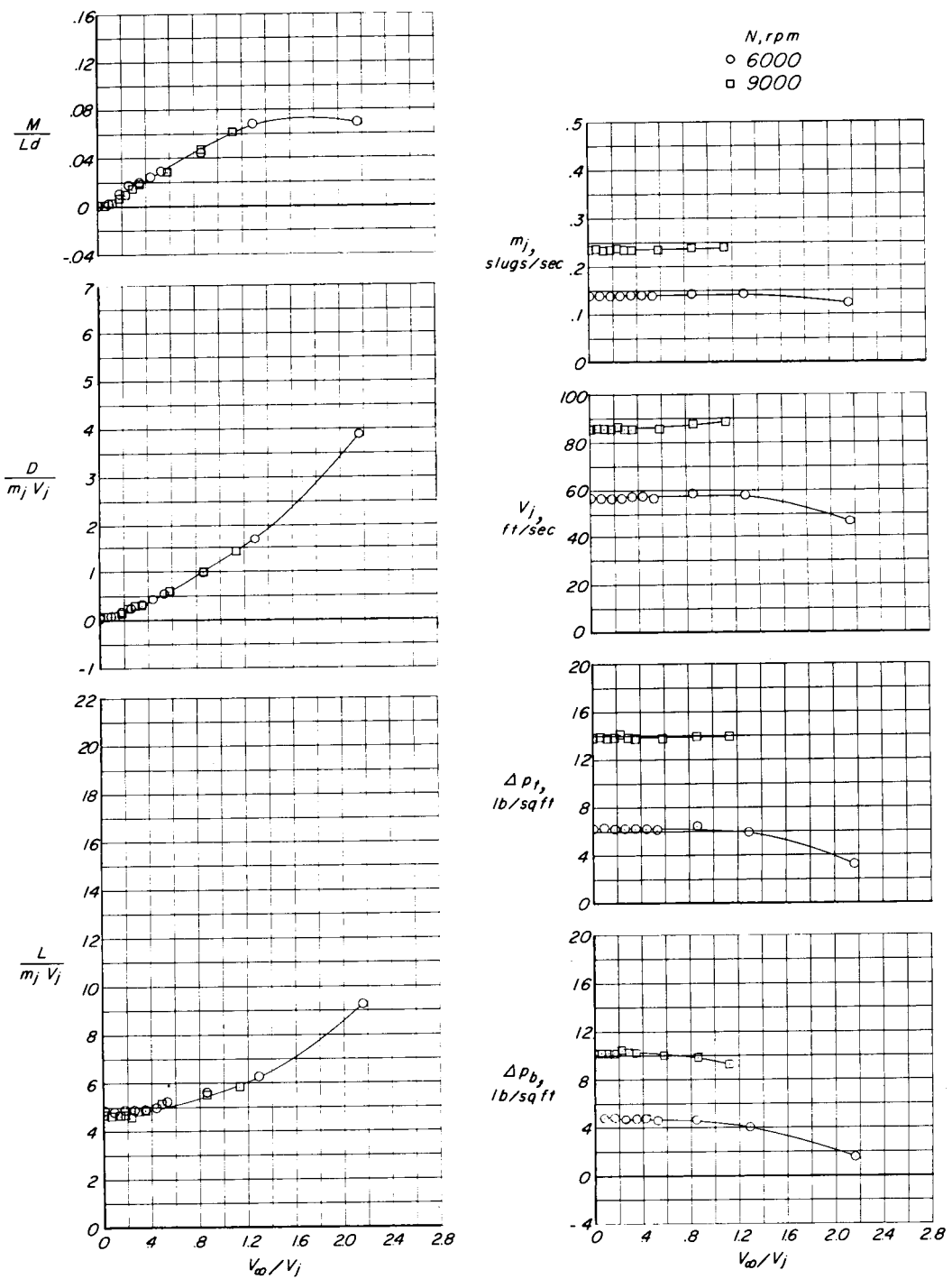
(f) h/d = 0.05.

Figure 4.- Continued.
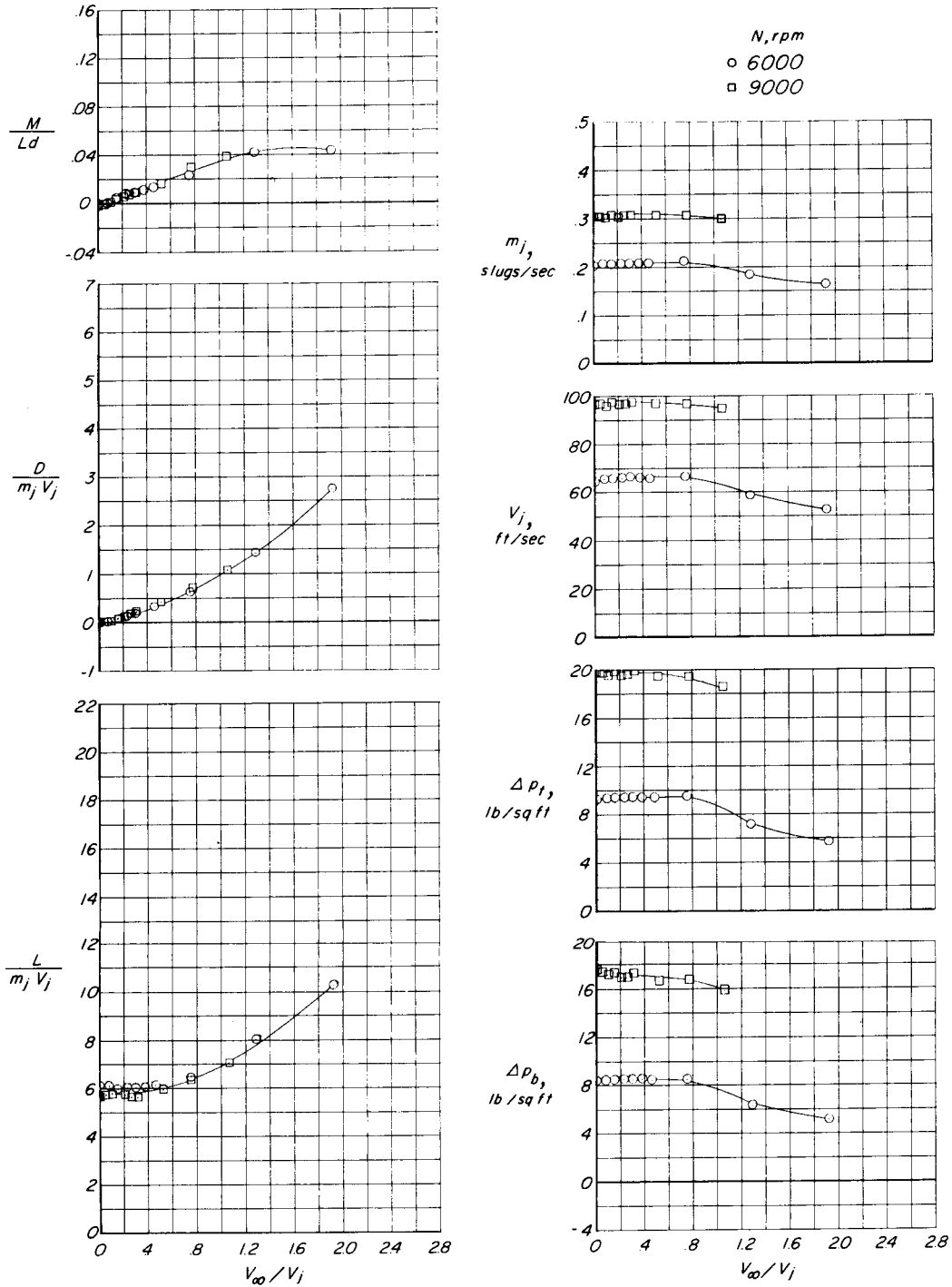
(g) h/d = 0.02.

Figure 4.- Concluded.
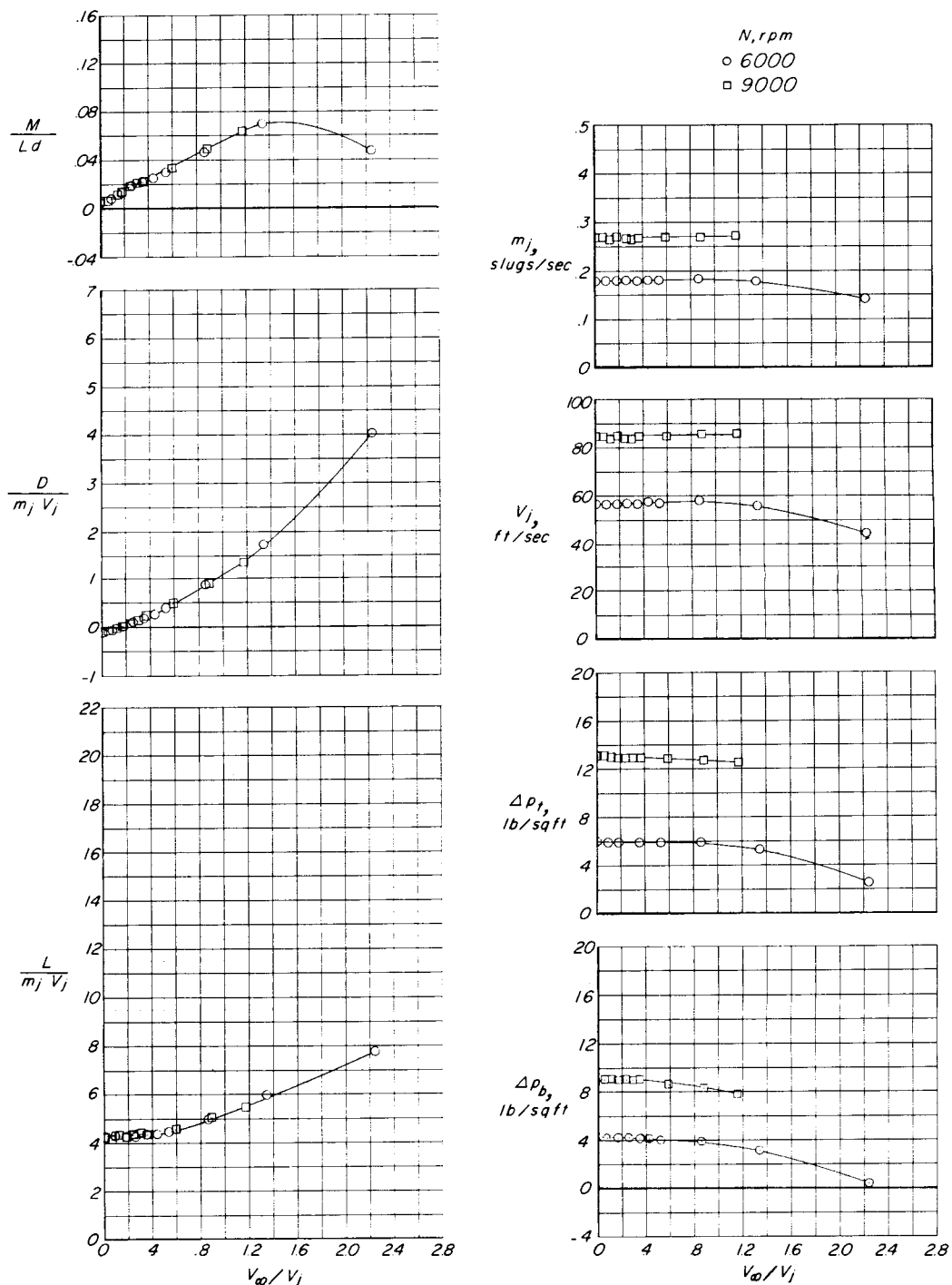
(a) α = -2°.

Figure 5.- Basic data as a function of velocity ratio at a height-diameter ratio of 0.05 for various angles of attack.

(b) α = -1°.
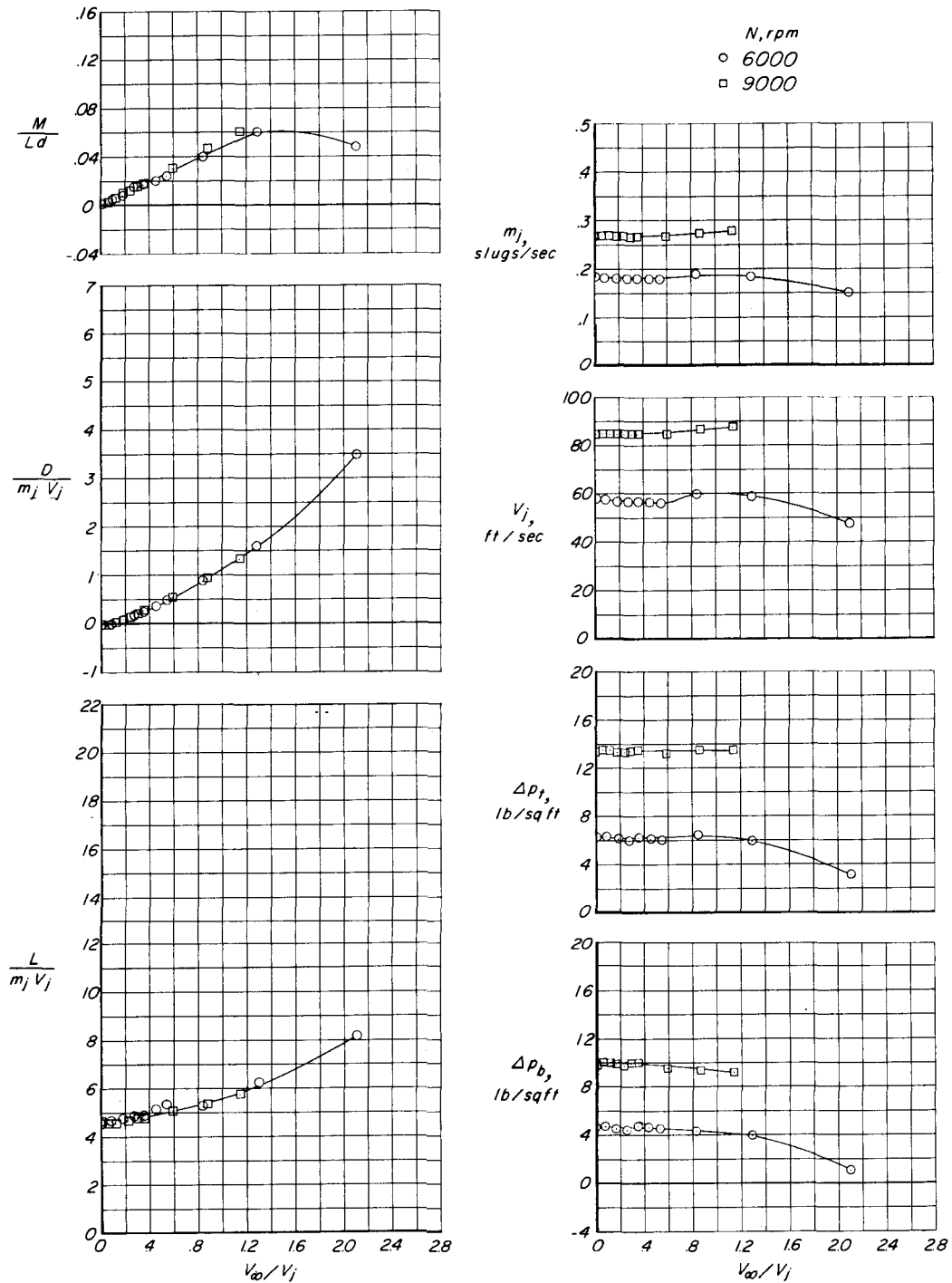
Figure 5.- Continued.
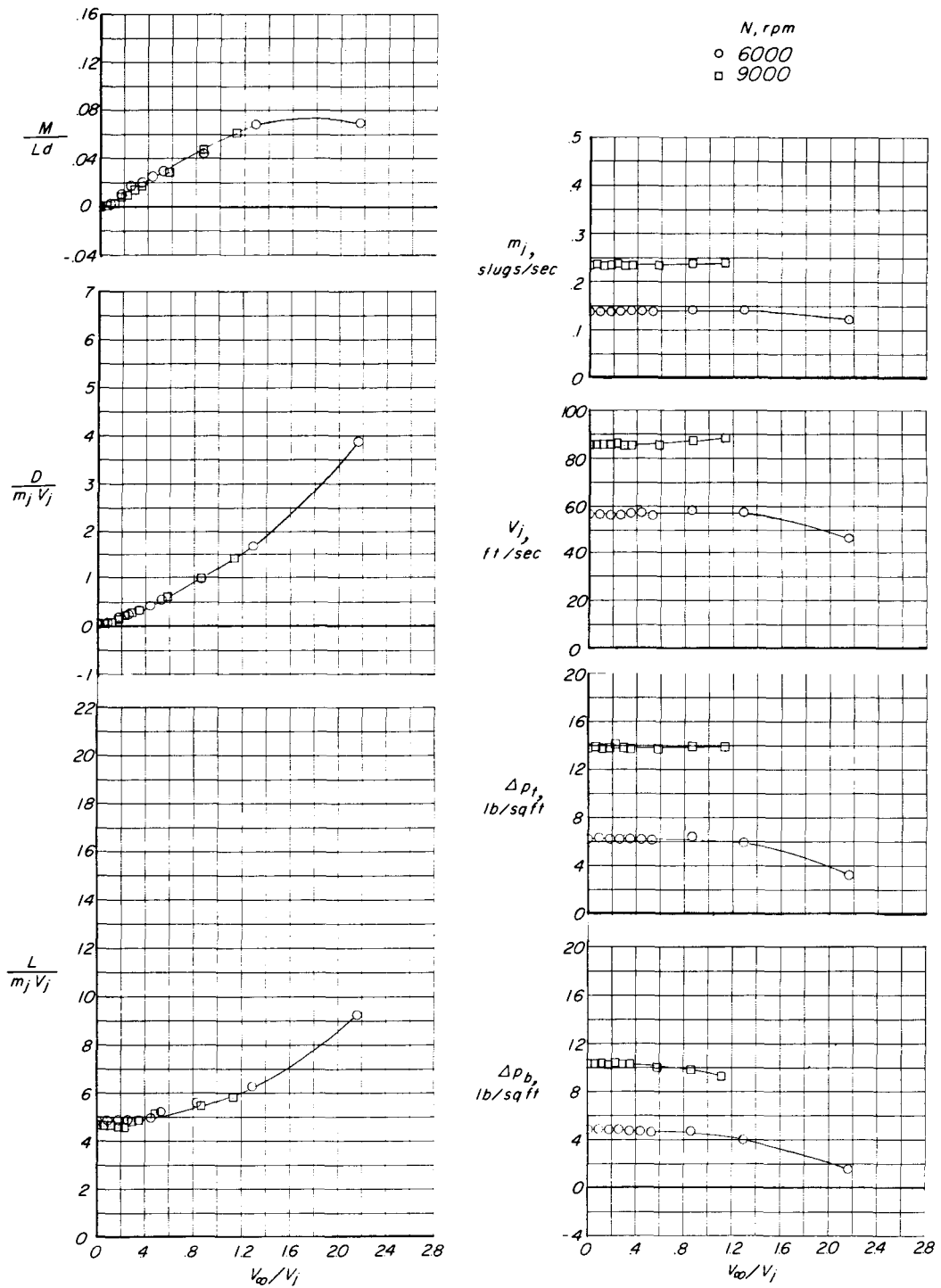
(c) α = 0°.

Figure 5.- Continued.
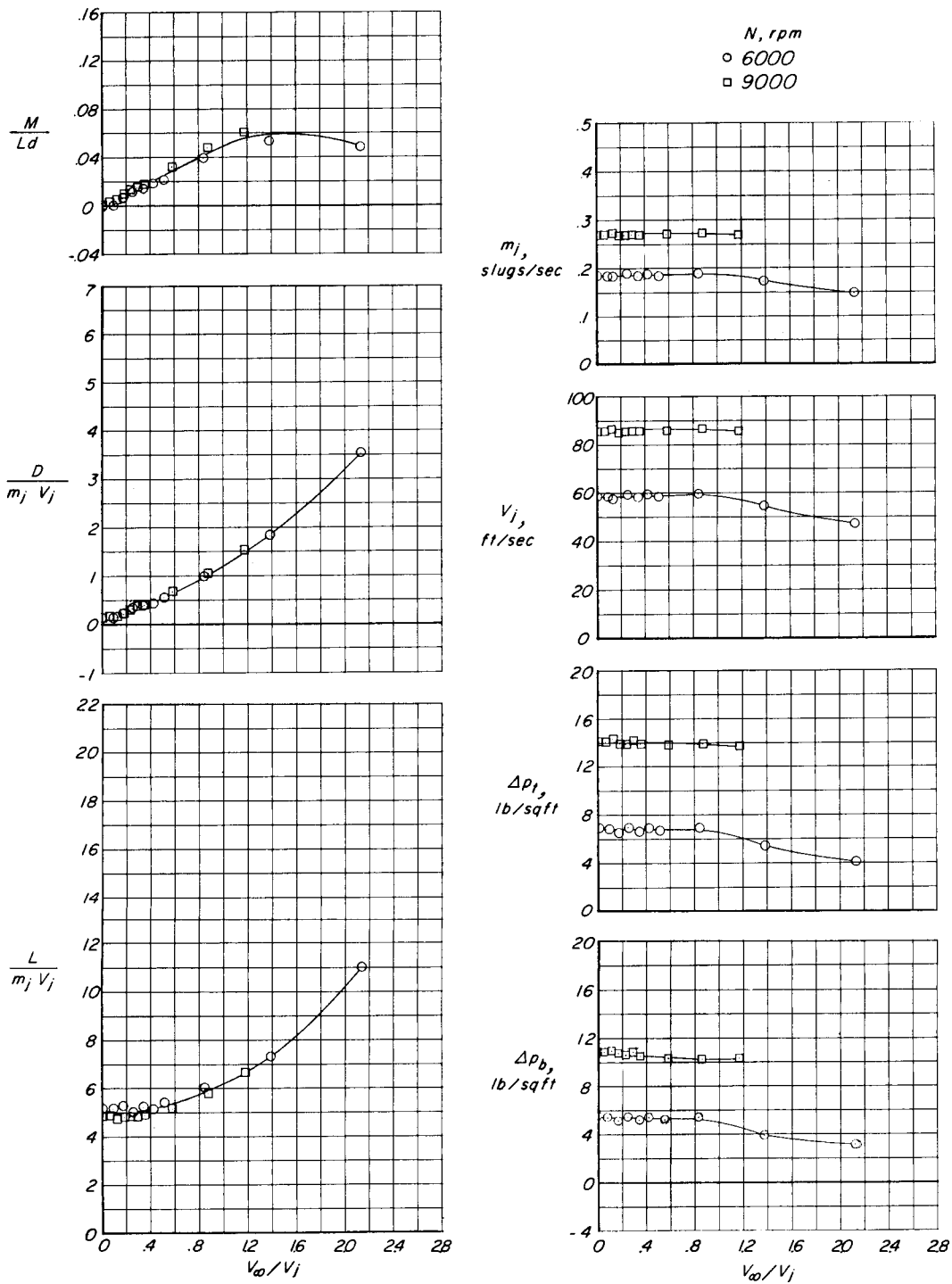
(d) $\alpha = 1°$.

Figure 5.- Continued.
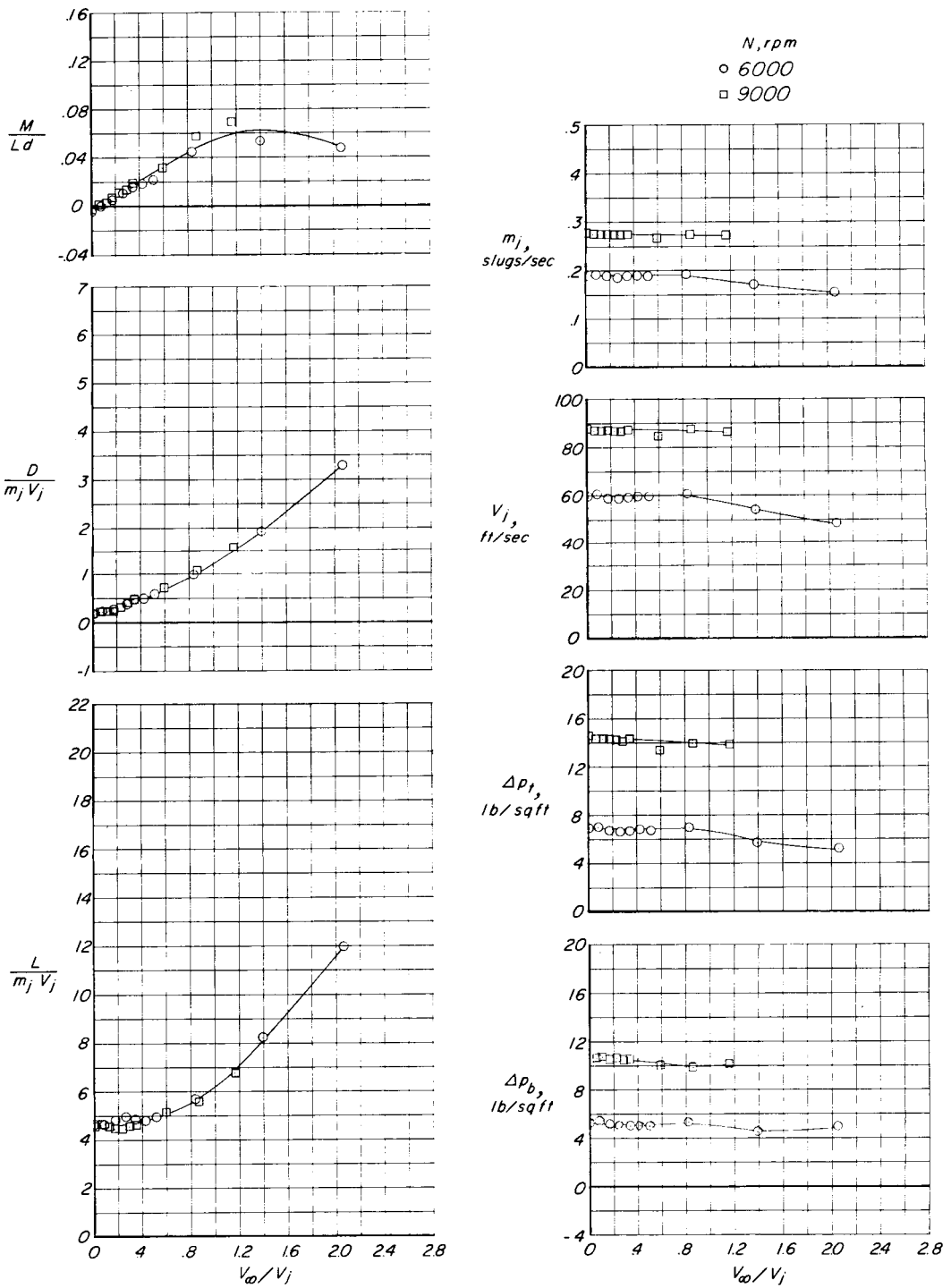
(e) $\alpha = 2°$.

Figure 5.- Concluded.
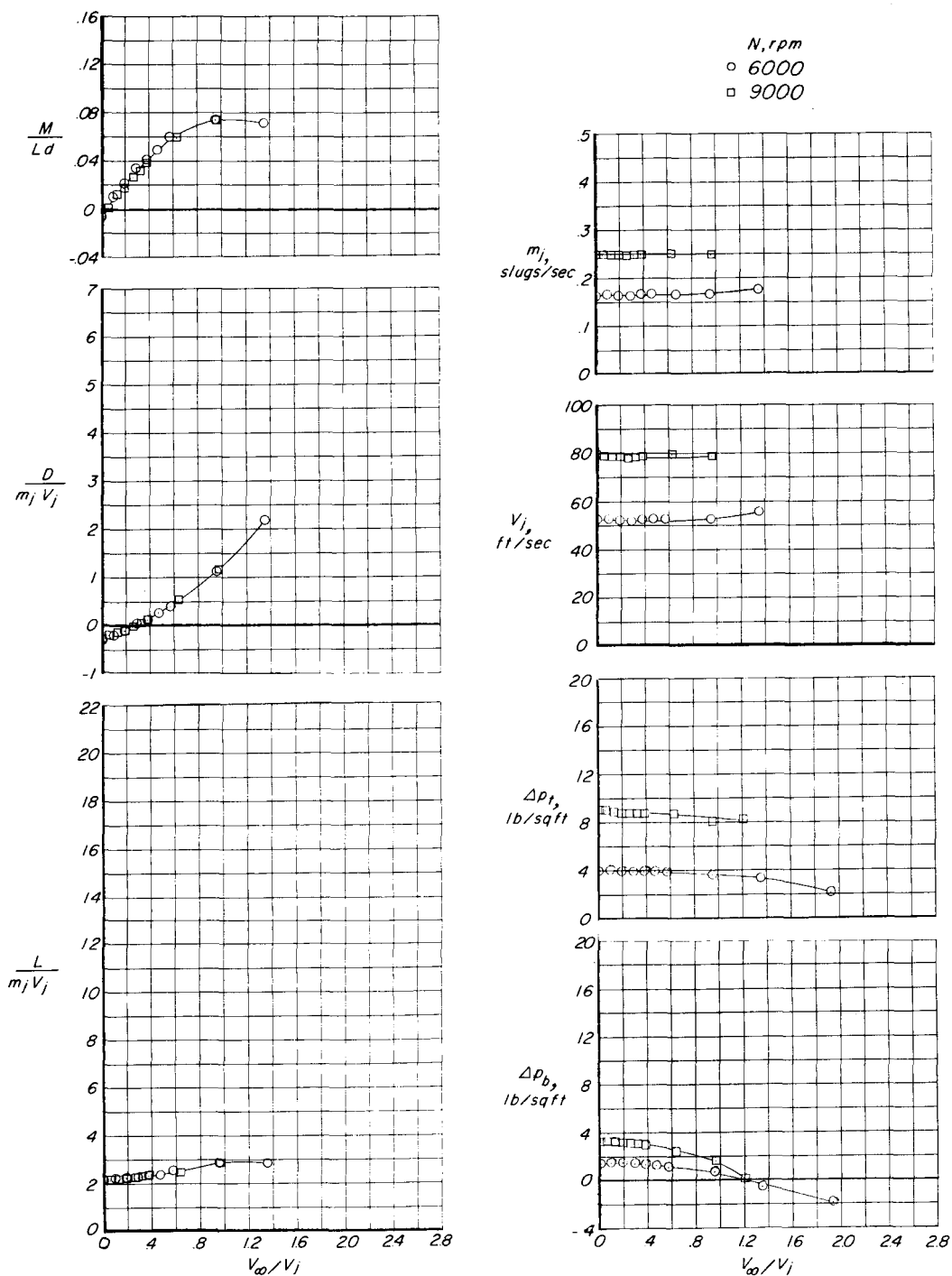
(a) α = -8°.

Figure 6.- Basic data as a function of velocity ratio at a height-diameter ratio of 0.10 for various angles of attack.

(b) α = -5°.
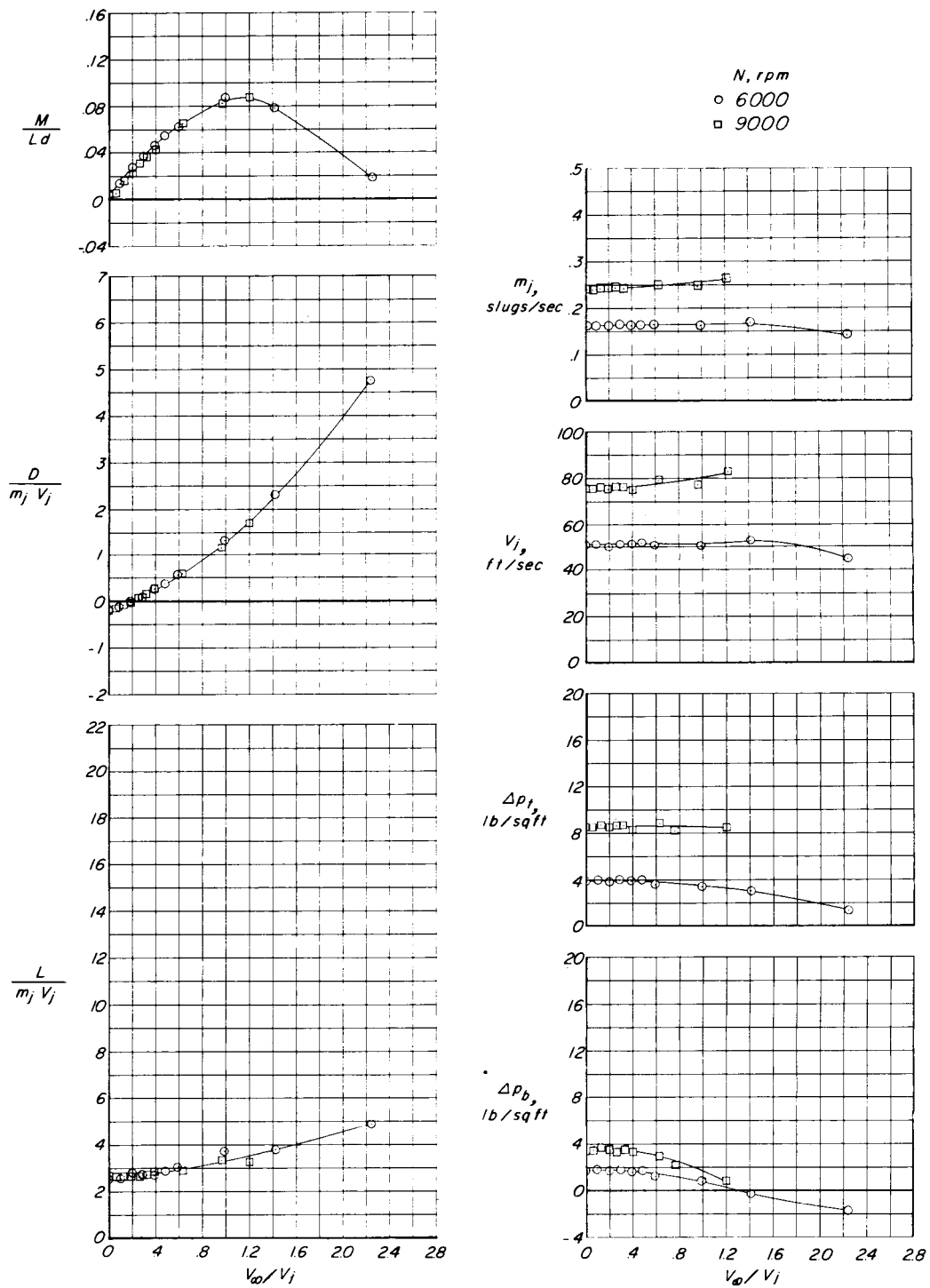
Figure 6.- Continued.

(c) α = -2°.
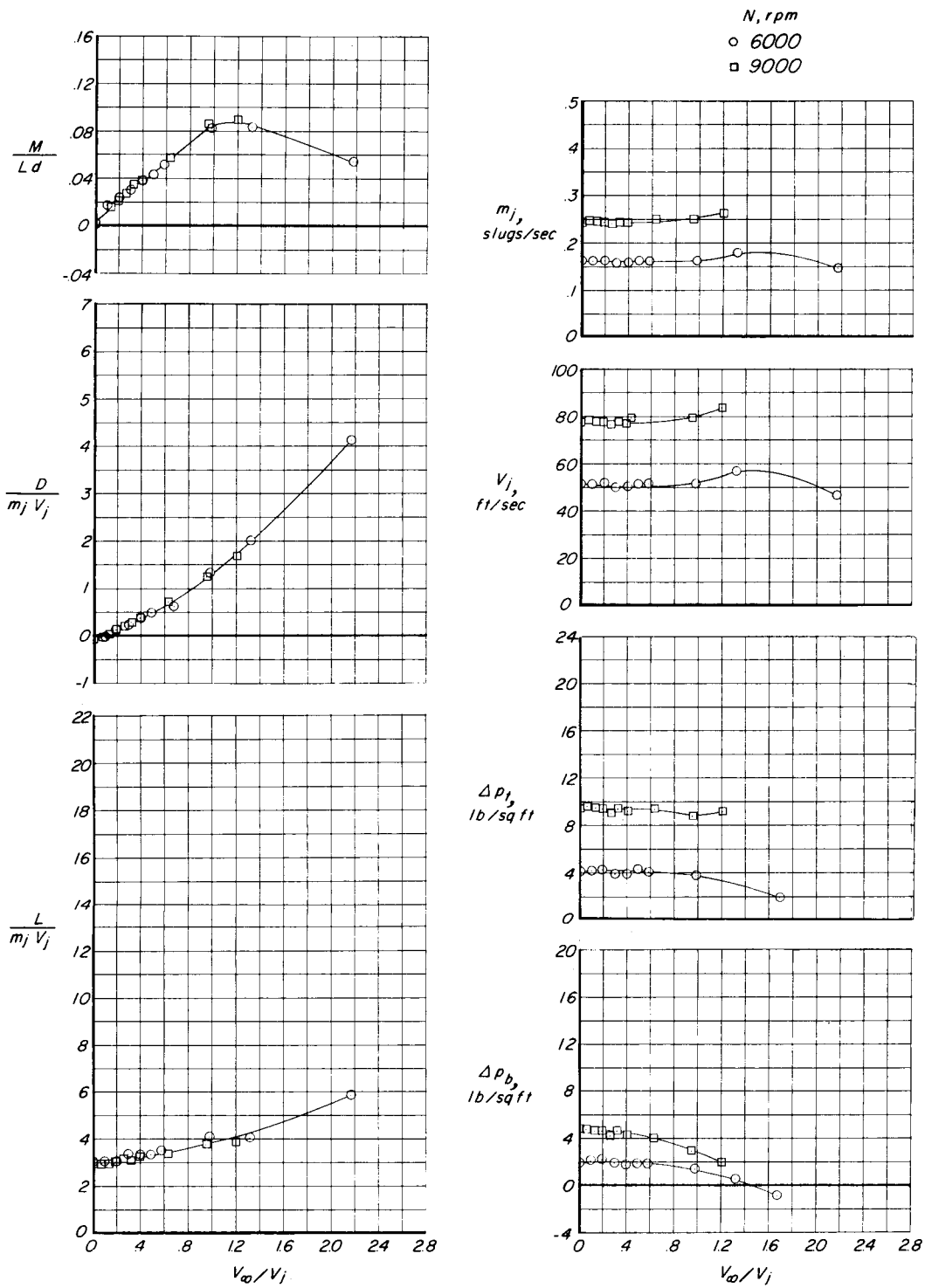
Figure 6.- Continued.
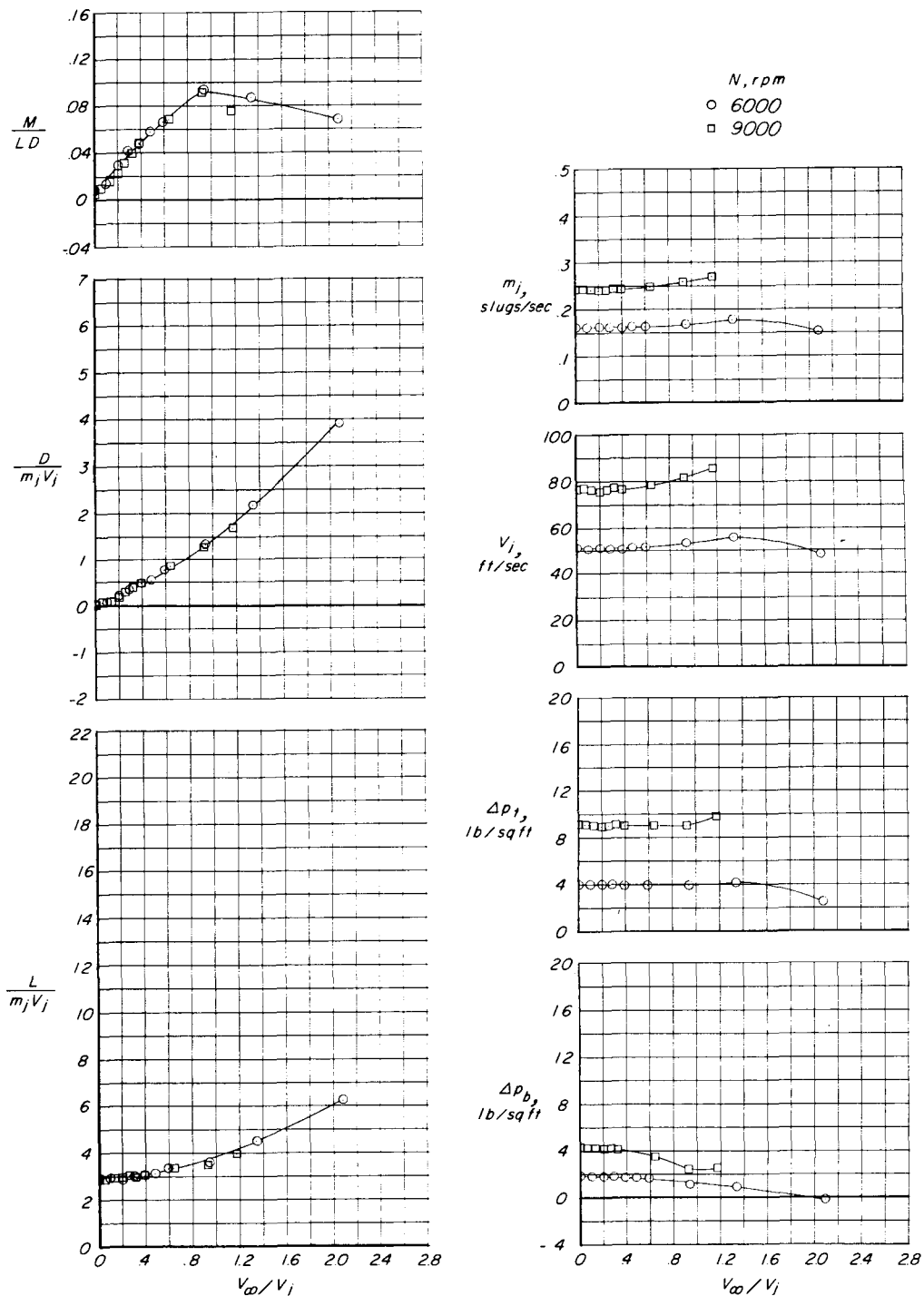
(d) α = 0°.

Figure 6.- Continued.

28
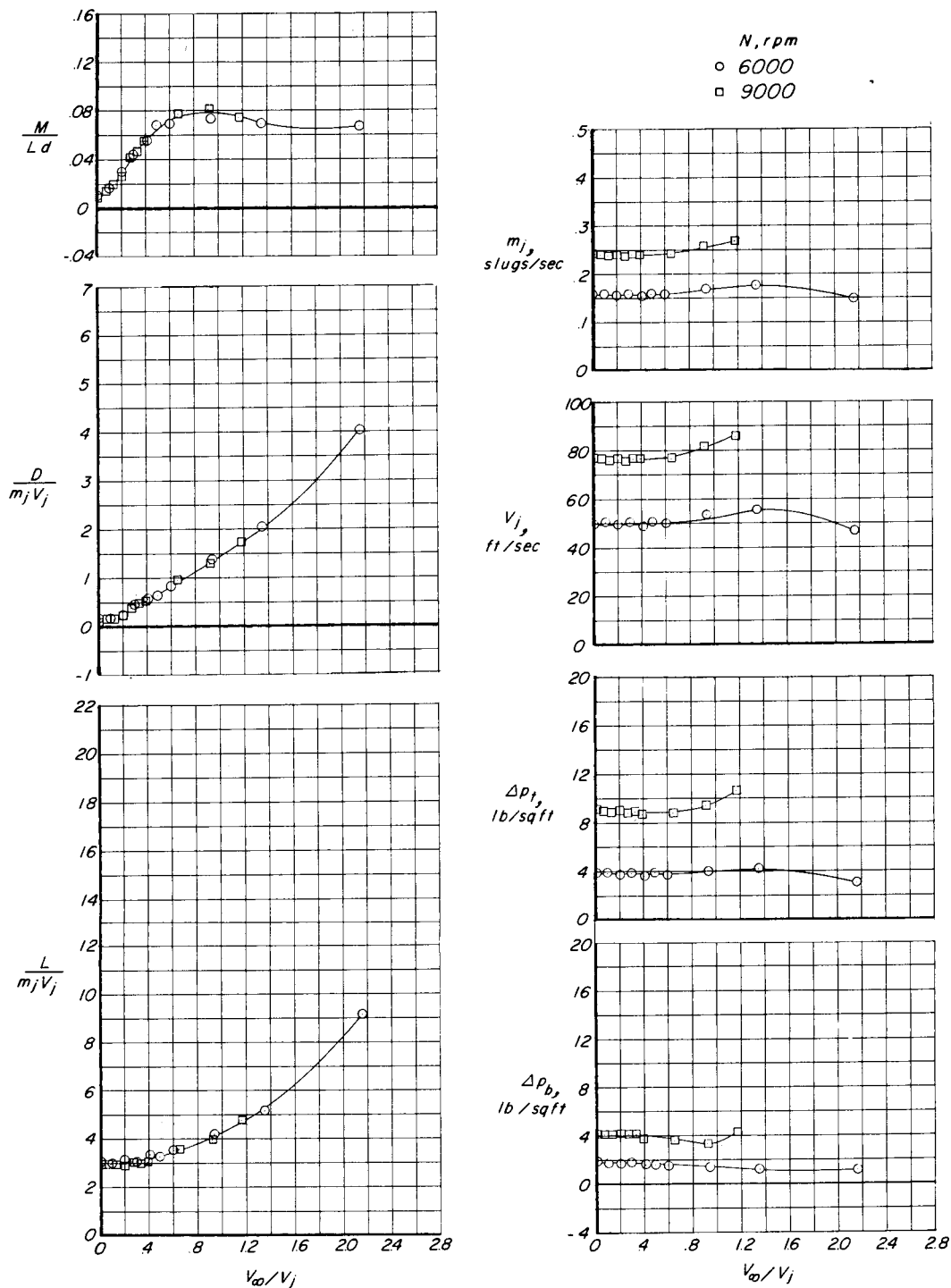
(e) $\alpha = 2°$.

Figure 6.- Continued.
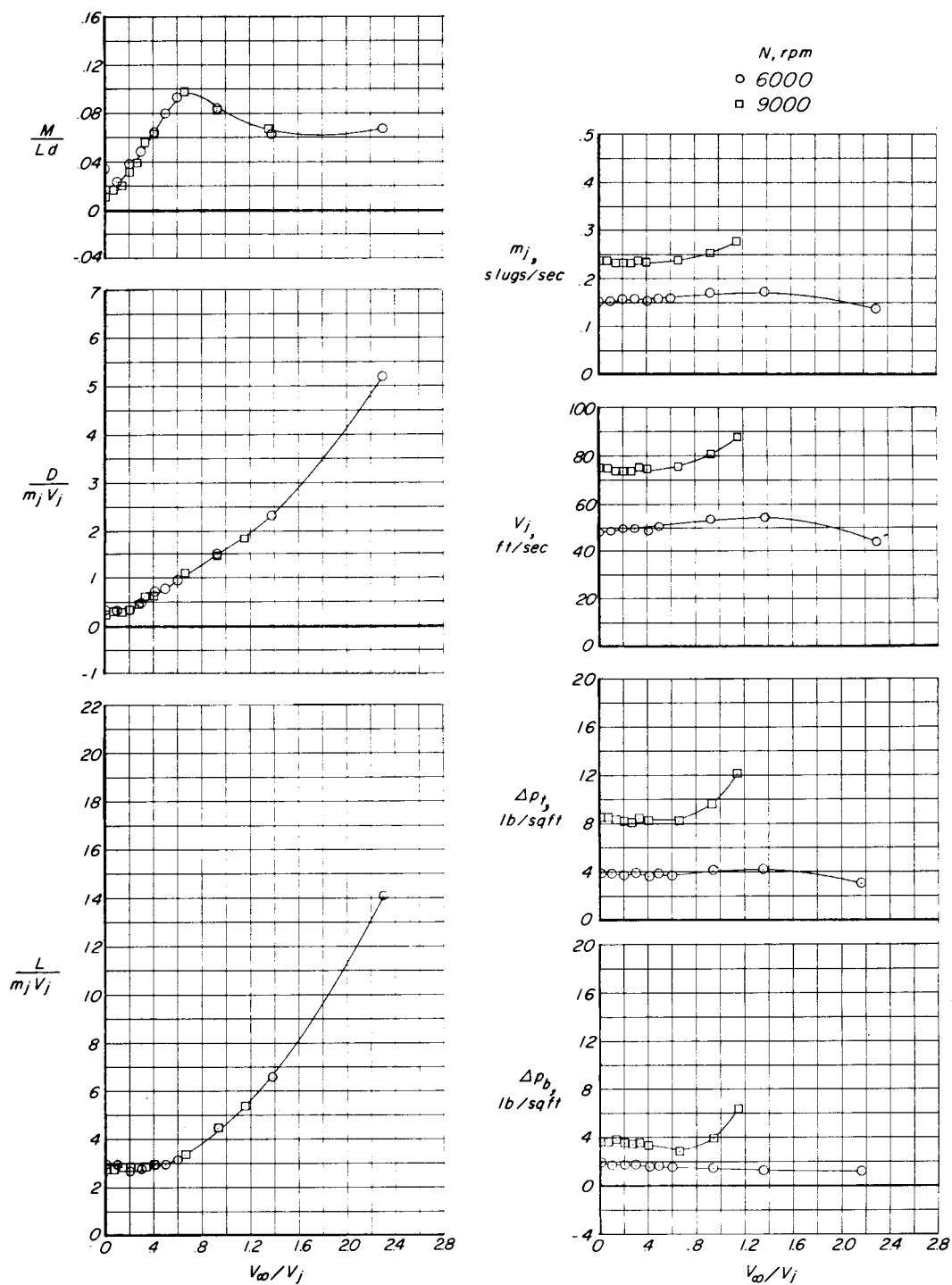
(f) $\alpha = 5°$.

Figure 6.- Continued.
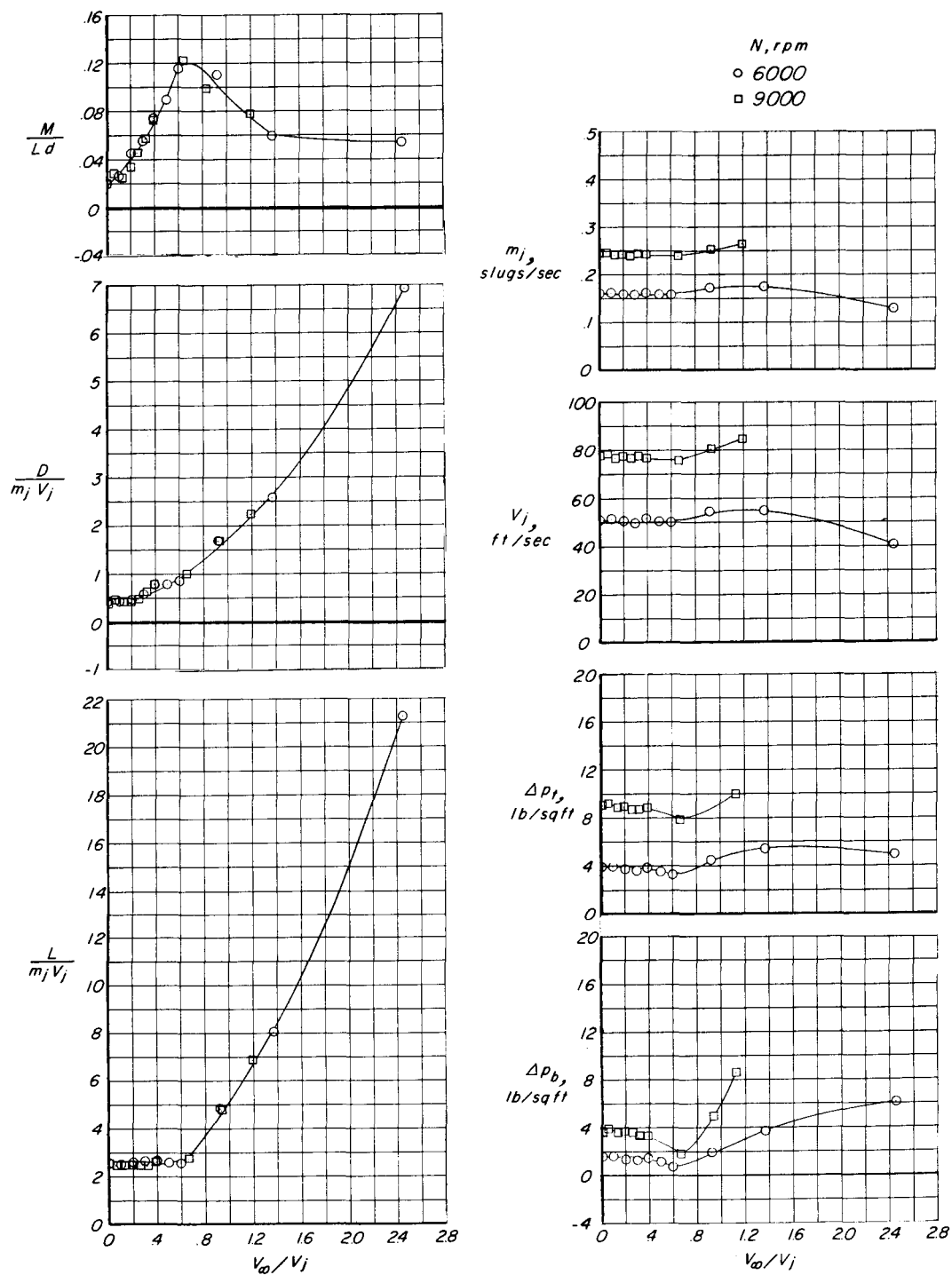
(g) $\alpha = 8°$.

Figure 6.- Concluded.
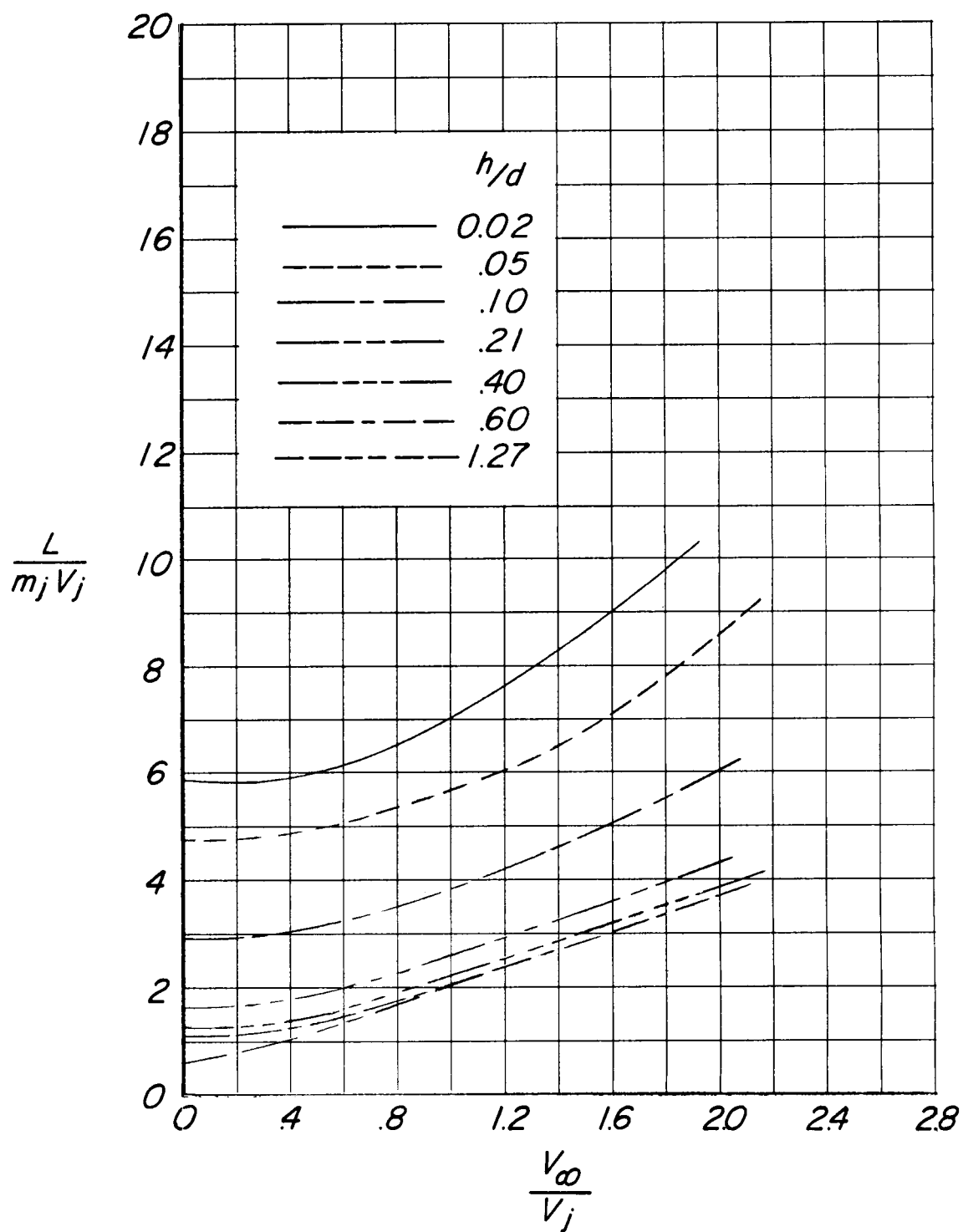
Figure 7.- Lift augmentation as a function of velocity ratio for various height-diameter ratios. $\alpha = 0^{\circ}$.
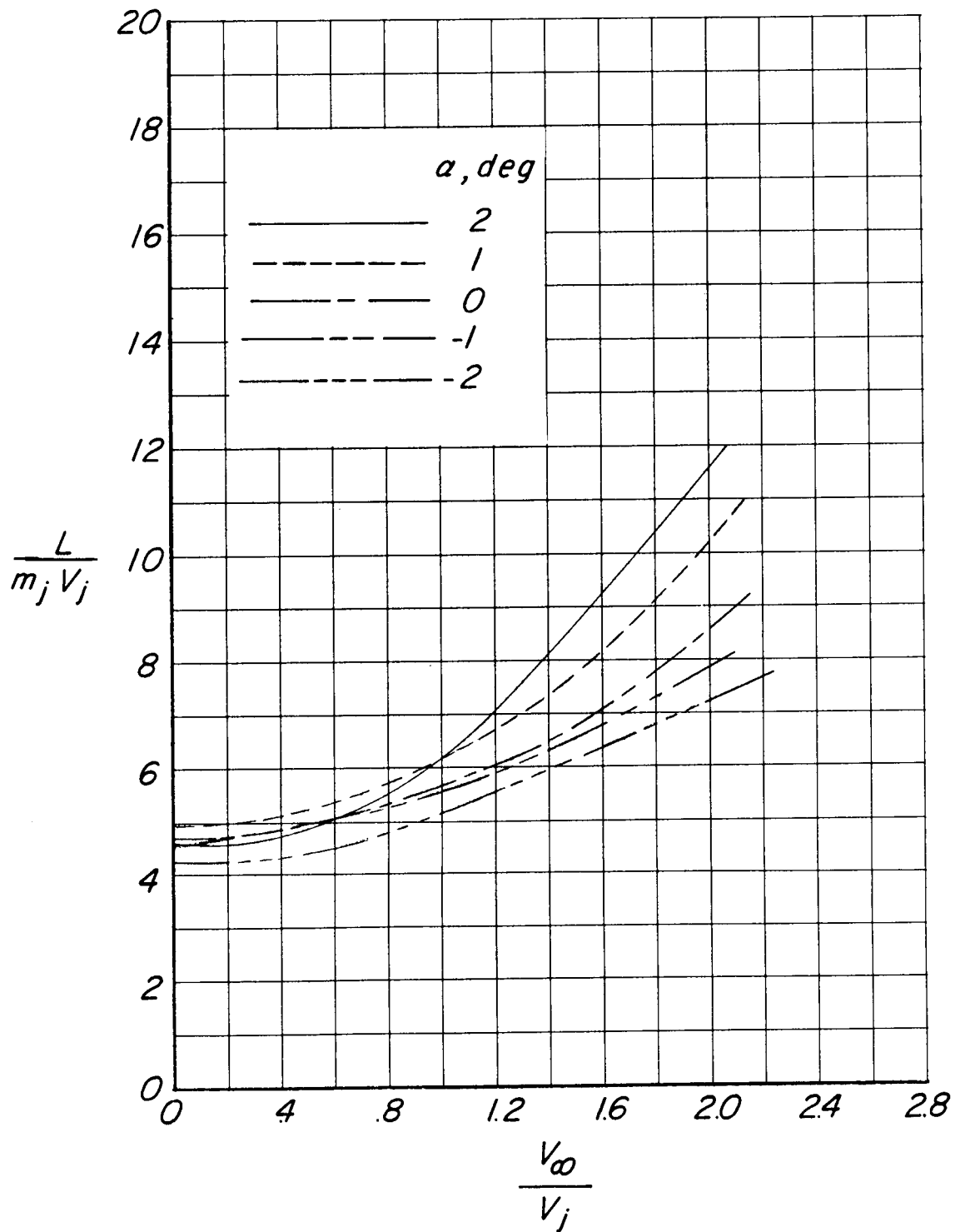
Figure 8.- Lift augmentation as a function of velocity ratio for various angles of attack.
h/d = 0.05.
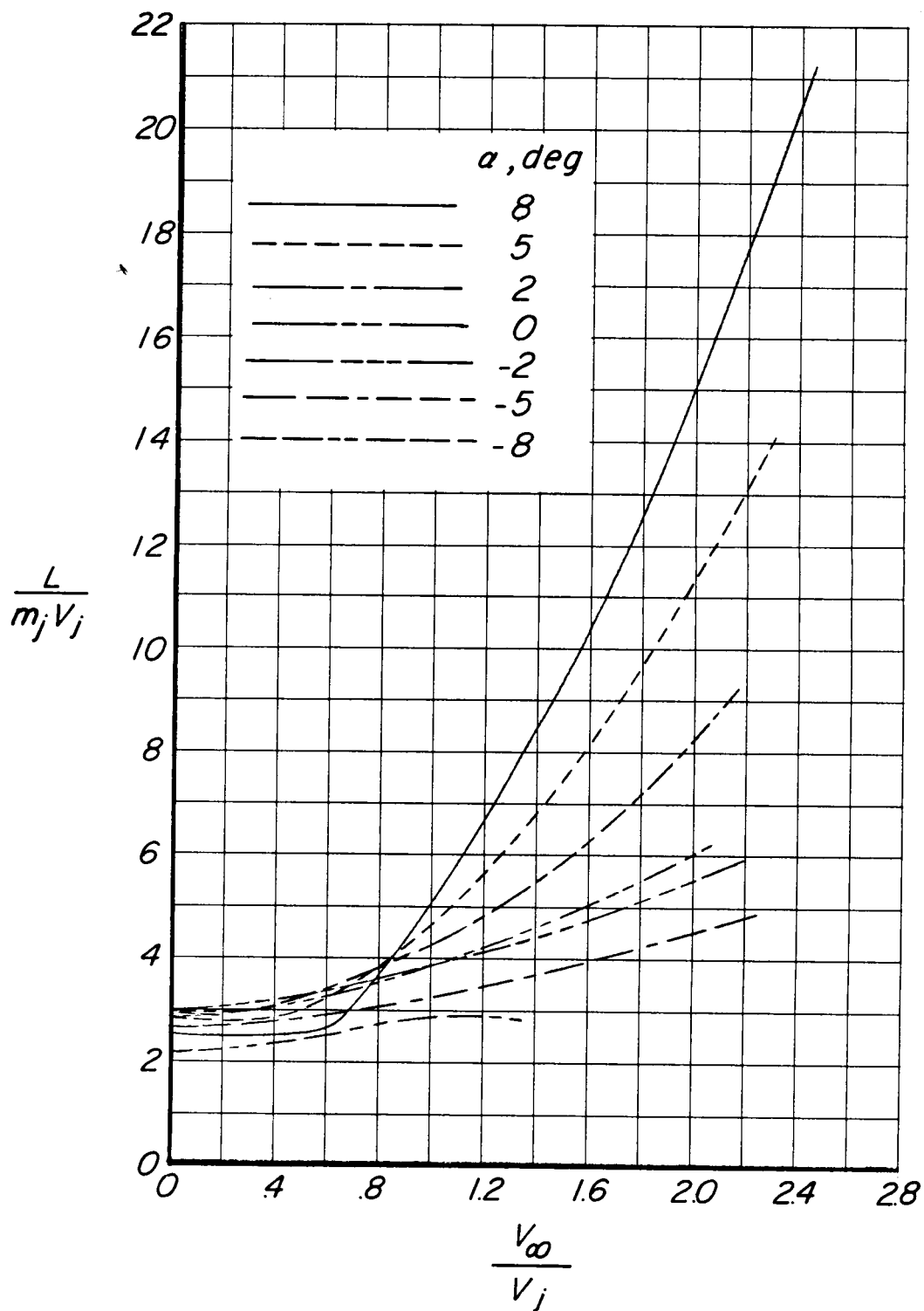
Figure 9.- Lift augmentation as a function of velocity ratio for various angles of attack. h/d = 0.10.
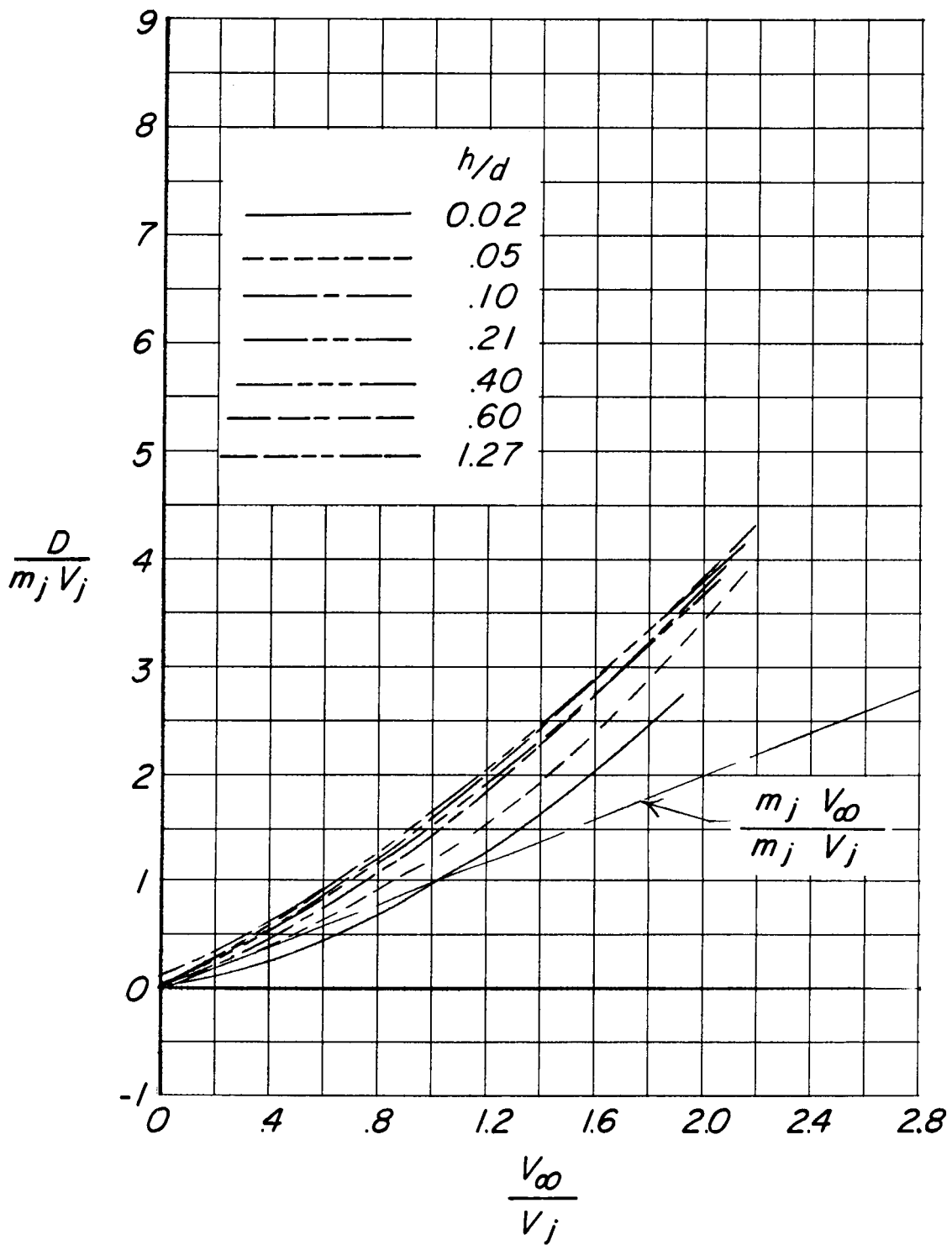
Figure 10.- Nondimensional drag parameter as a function of velocity ratio for various height-diameter ratios. $\alpha = 0°$.
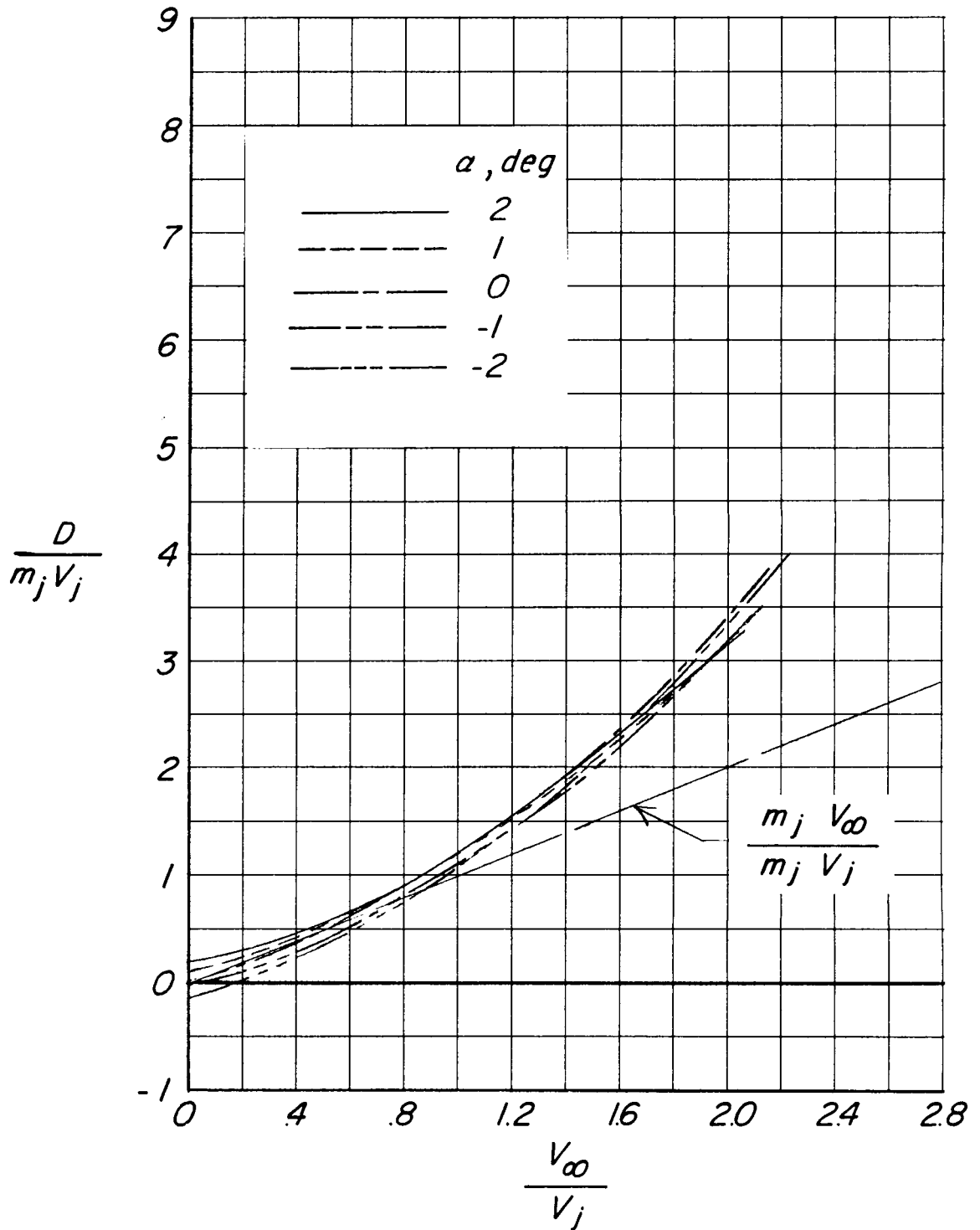
Figure 11.- Nondimensional drag parameter as a function of velocity ratio for various angles of attack. h/d = 0.05.
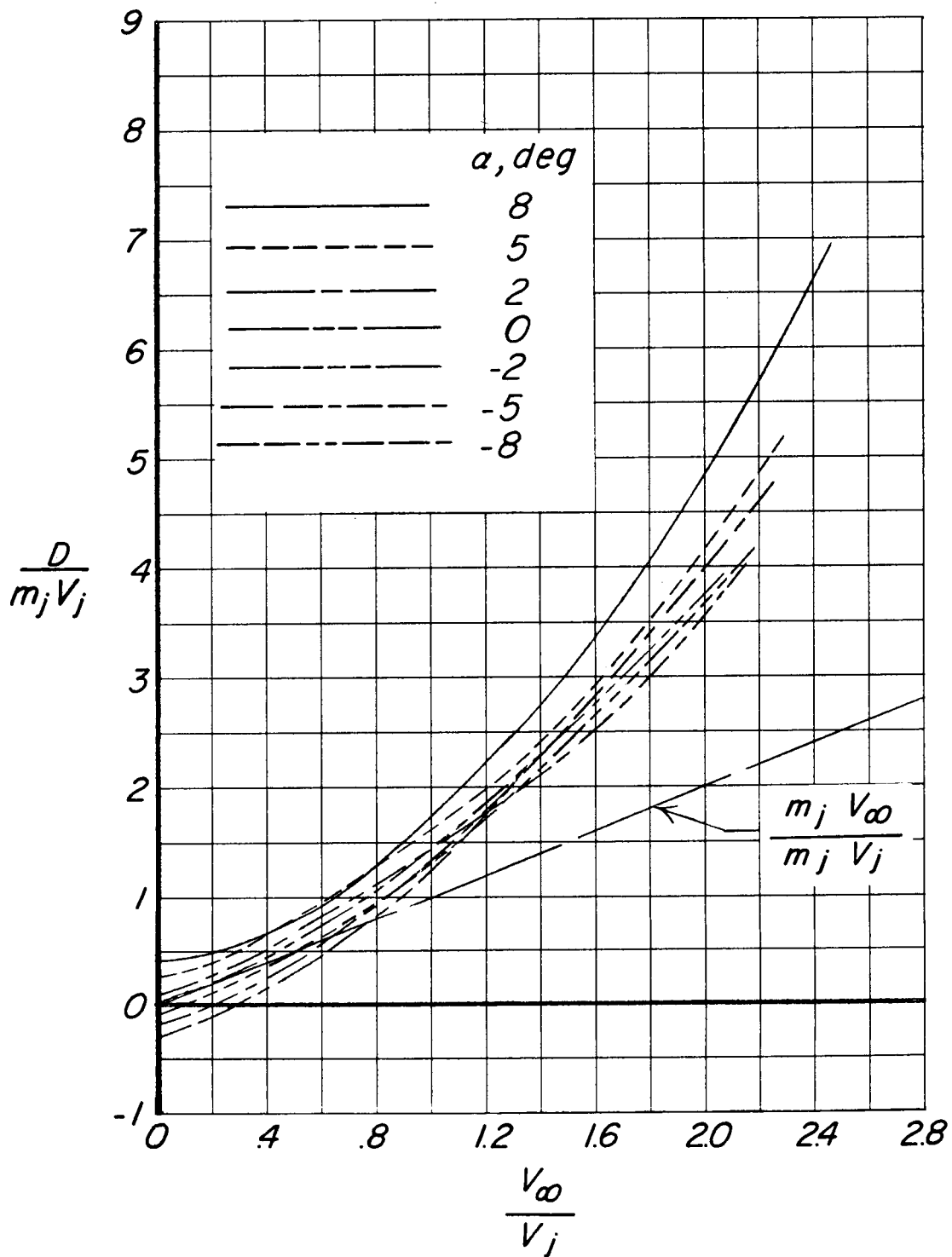
Figure 12.- Nondimensional drag parameter as a function of velocity ratio for various angles of attack. $h/d = 0.10$.
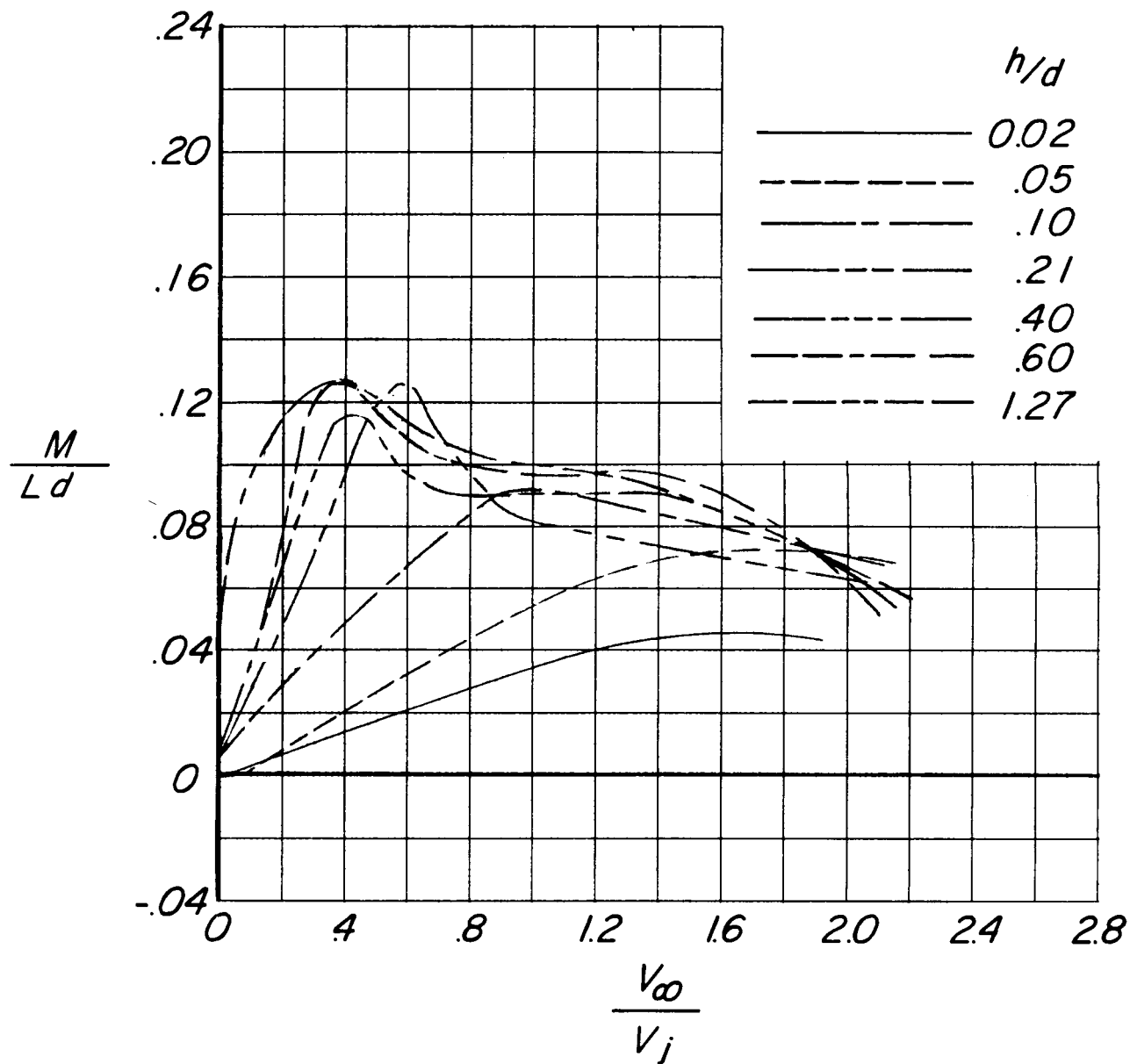
Figure 13.- Nondimensional pitching-moment parameter as a function of velocity ratio for various height-diameter ratios. $\alpha = 0^\circ$.
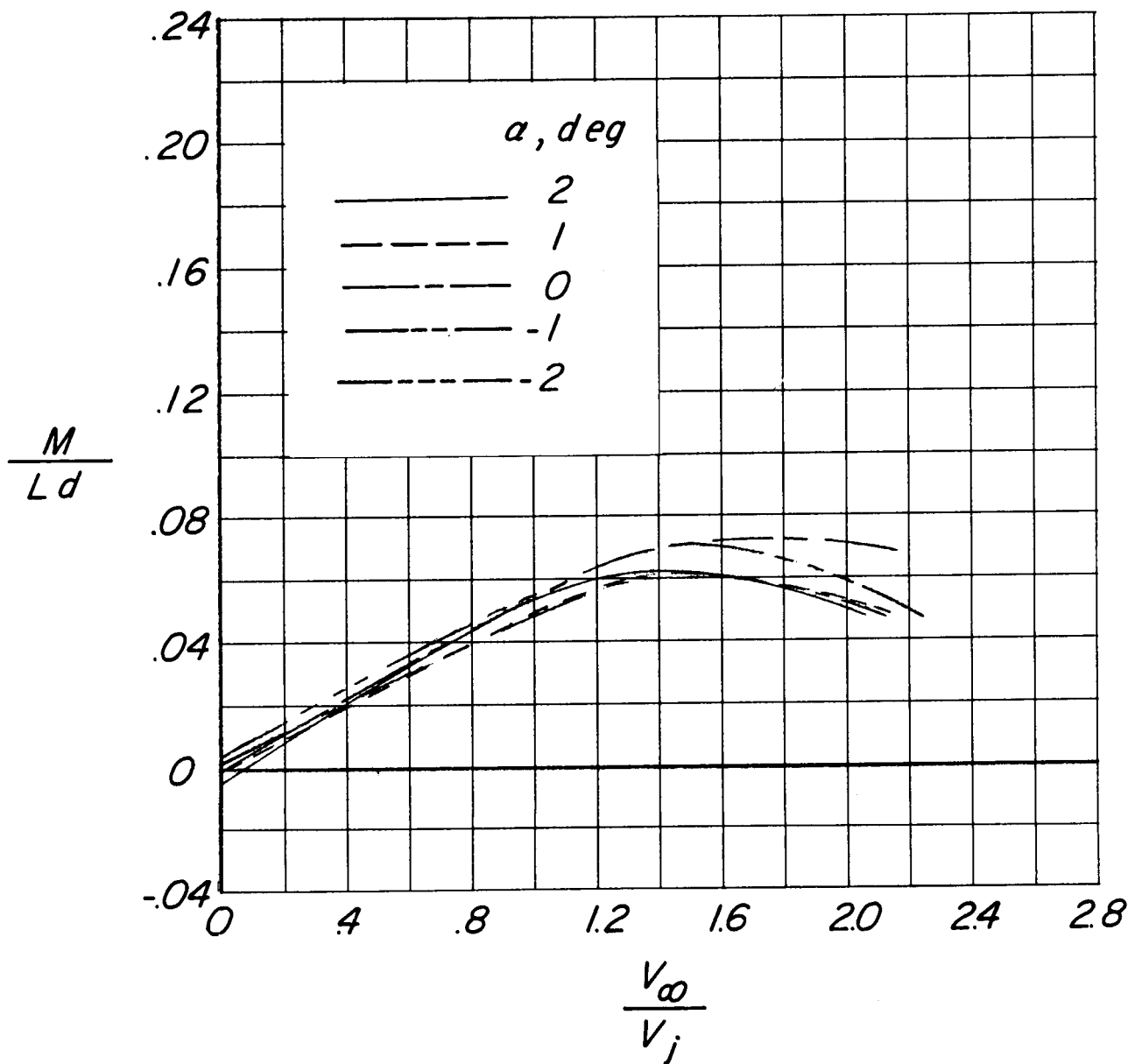
Figure 14.- Nondimensional pitching-moment parameter as a function of velocity ratio for various angles of attack. h/d = 0.05.
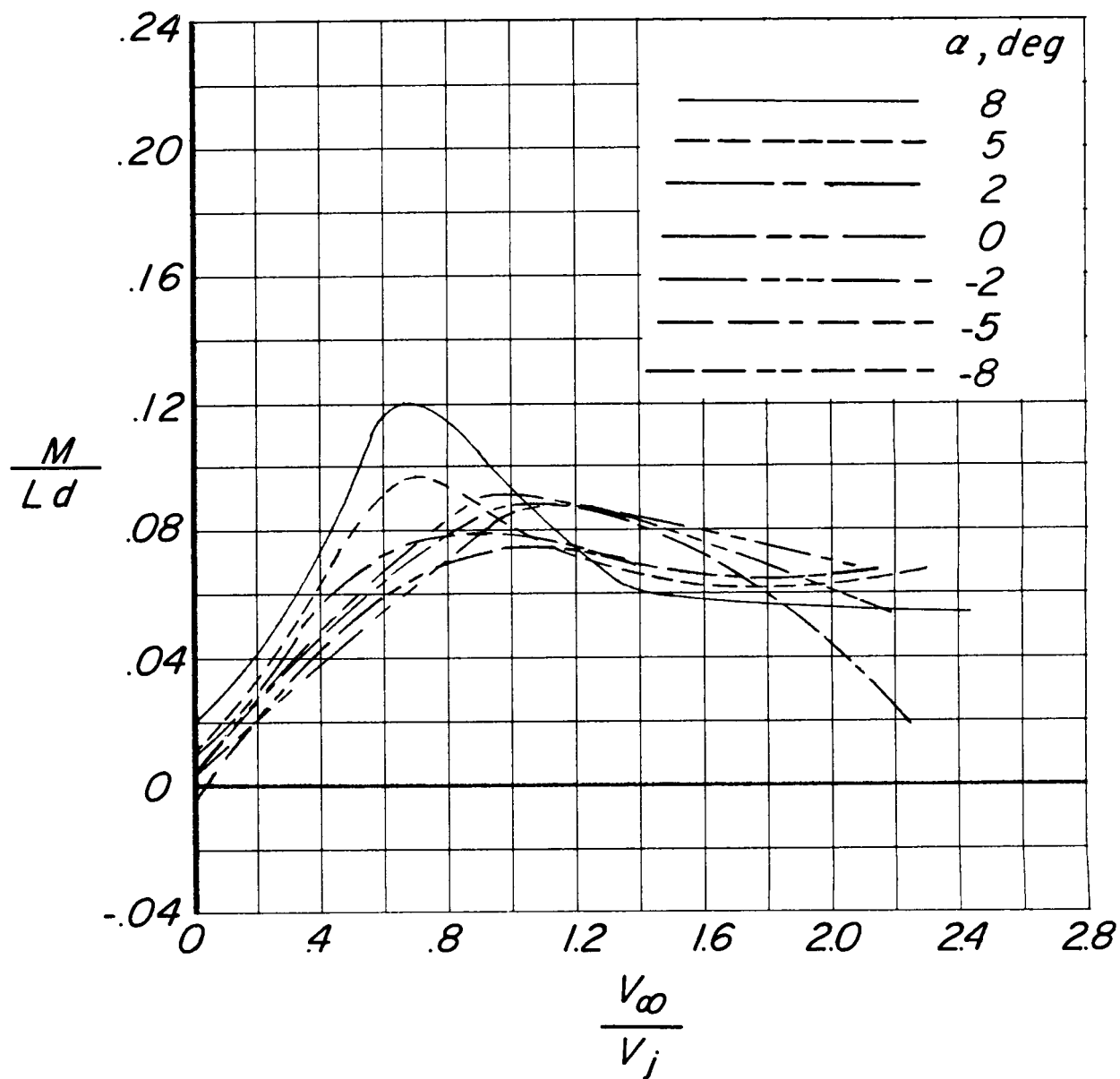
Figure 15.- Nondimensional pitching-moment parameter as a function of velocity ratio for various angles of attack. h/d = 0.10.

$$\frac{V_{\infty}}{V_j} = 0$$

V_{∞}

$$\frac{V_{\infty}}{V_j} = .18$$
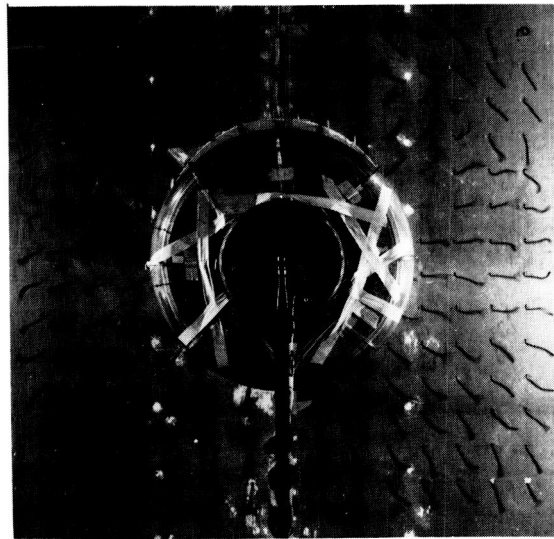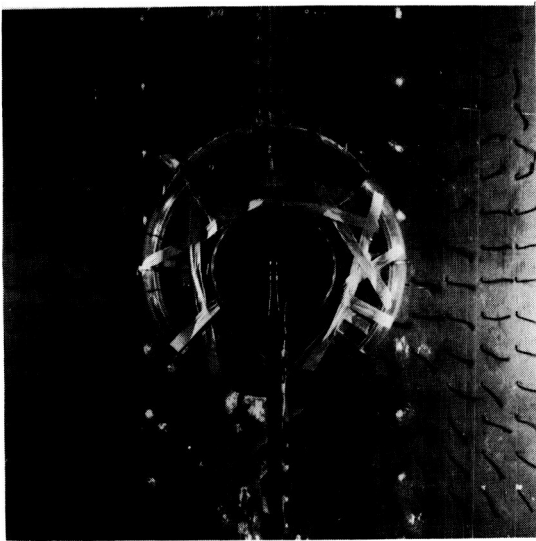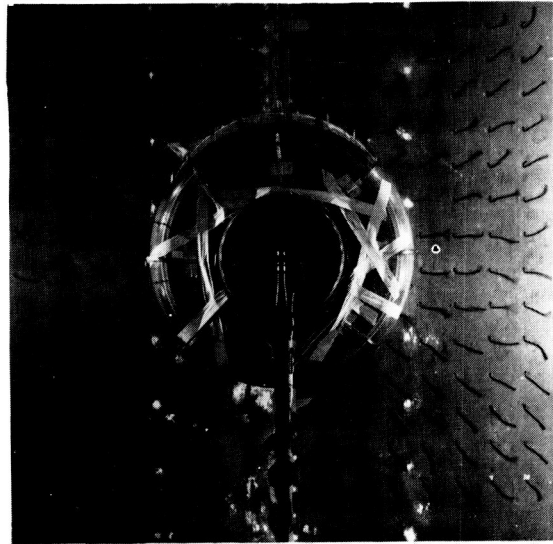
$$\frac{V_{\infty}}{V_j} = .35$$
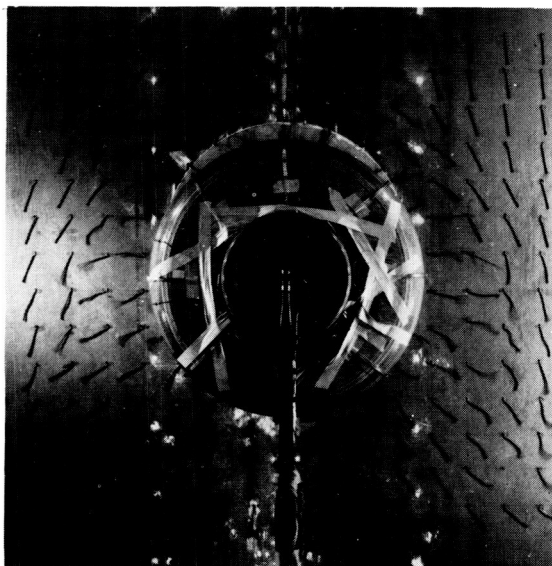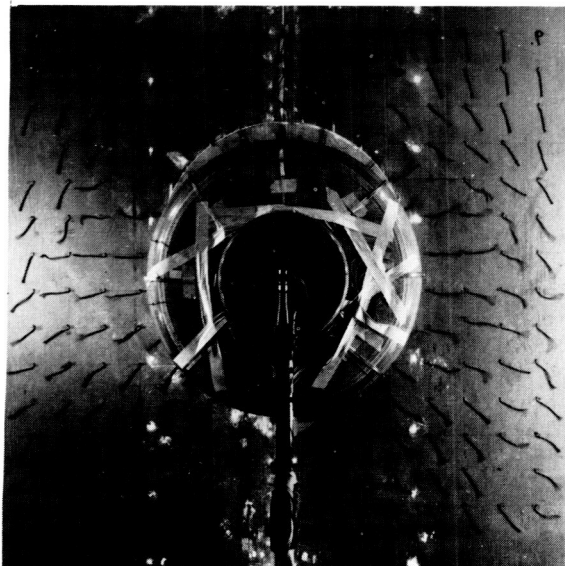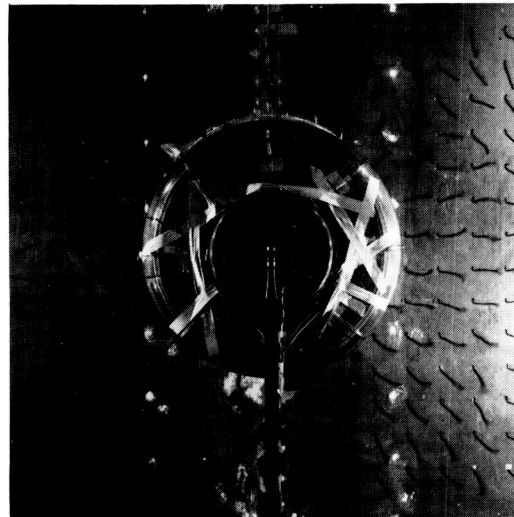
$$\frac{V_{\infty}}{V_j} = .44$$

L-63-24

Figure 16.- Photographs of tufts showing flow patterns at ground plane for various velocity ratios. α = 0°; h/d = 0.05.

$$\frac{V_\infty}{V_j} = .53$$

V_∞
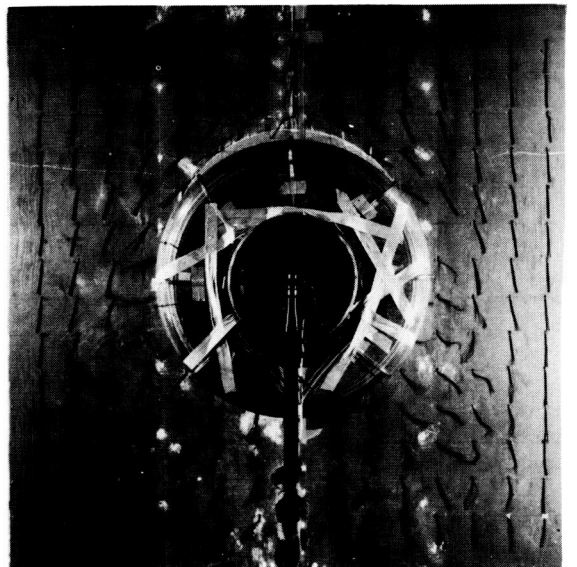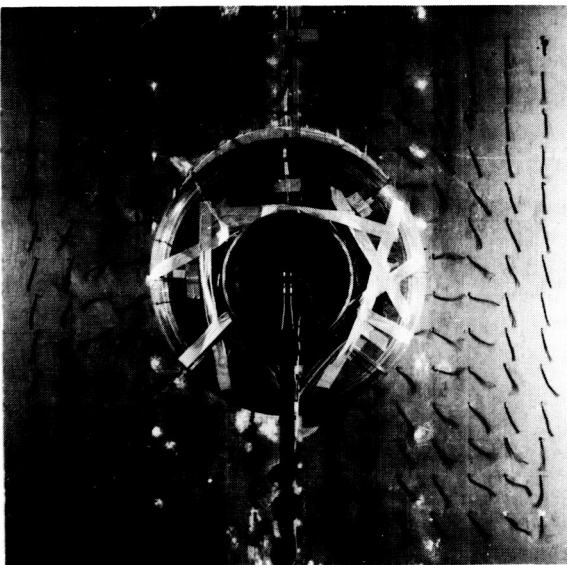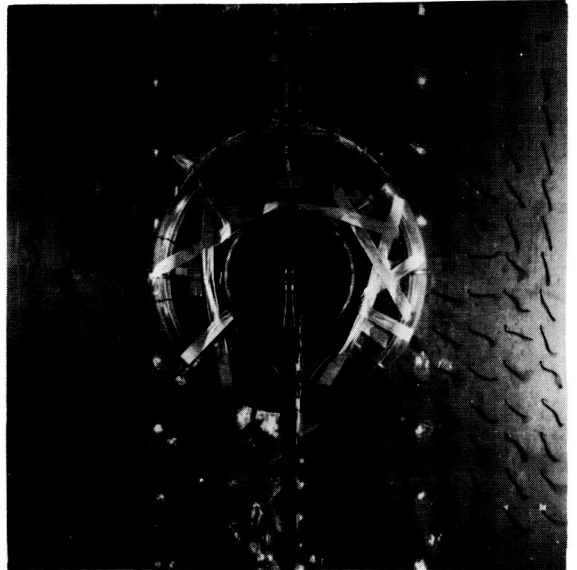
$$\frac{V_\infty}{V_j} = .86$$

$$\frac{V_\infty}{V_j} = 1.29$$
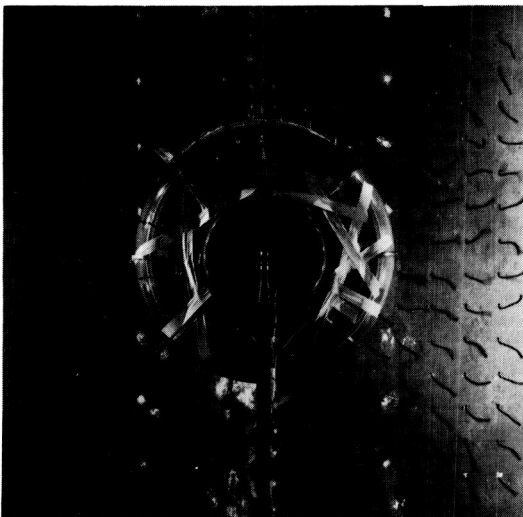
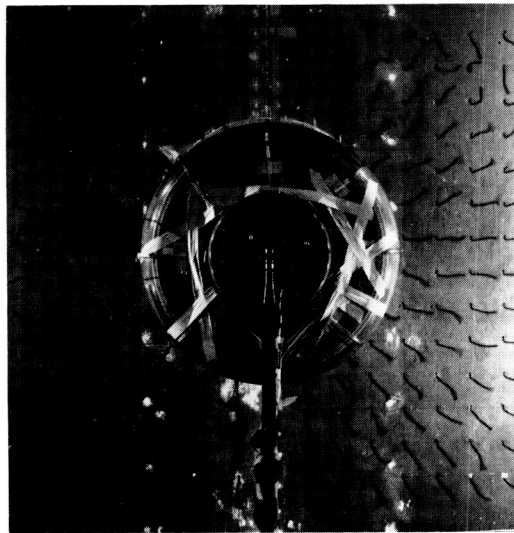$$\frac{V_\infty}{V_j} = 2.16$$

Figure 16.- Concluded.

L-63-25

$$\frac{V_\infty}{V_j} = 0$$

V_∞

$$\frac{V_\infty}{V_j} = .18$$
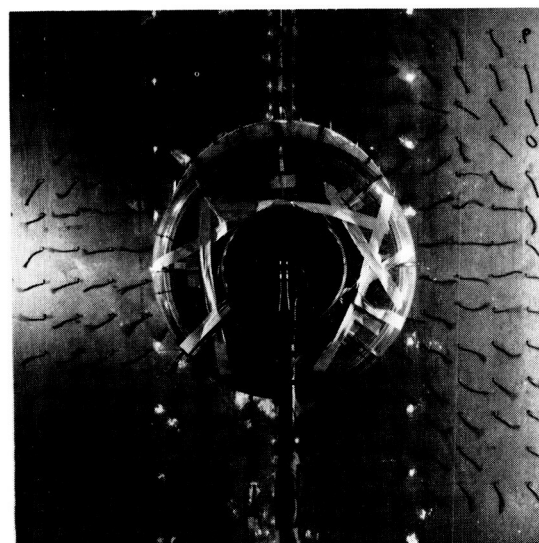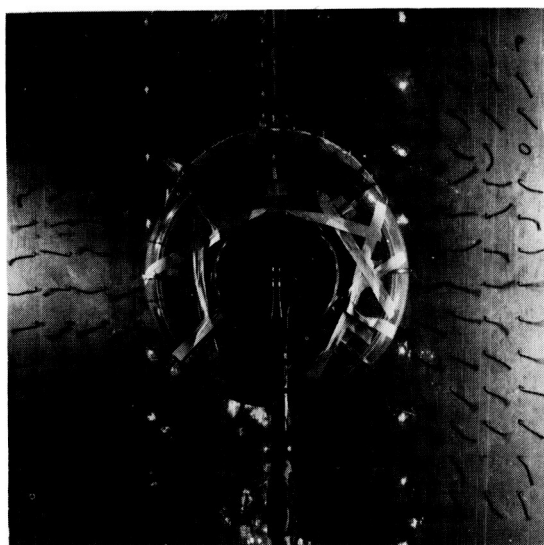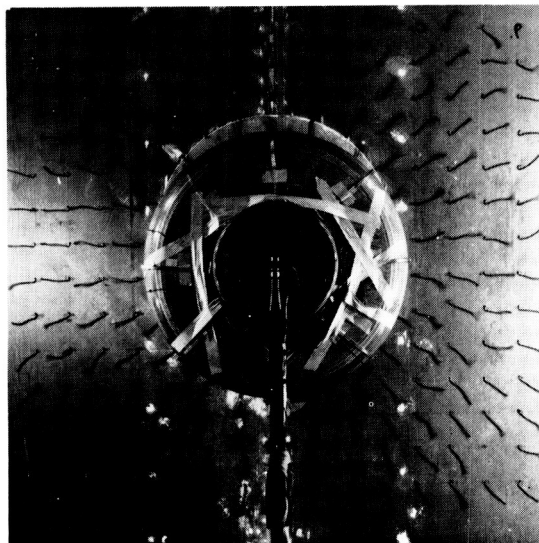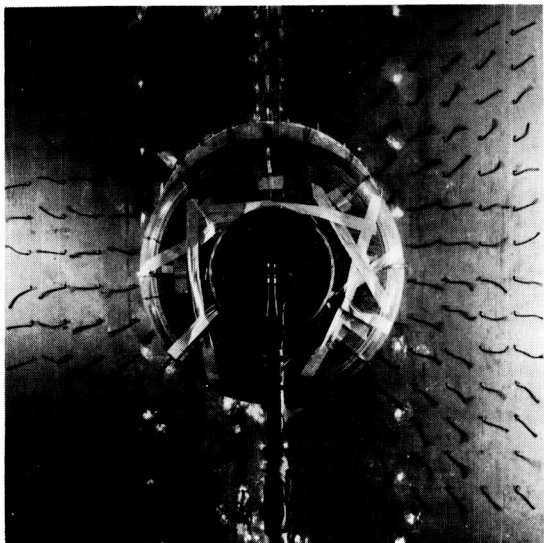
$$\frac{V_\infty}{V_j} = .35$$

$$\frac{V_\infty}{V_j} = .44$$

L-63-26

Figure 17.- Photographs of tufts showing flow patterns at ground plane for various velocity ratios. $\alpha = -2^\circ$; h/d = 0.05.

$$\frac{V_\infty}{V_j} = .53$$

V_∞

$$\frac{V_\infty}{V_j} = .86$$
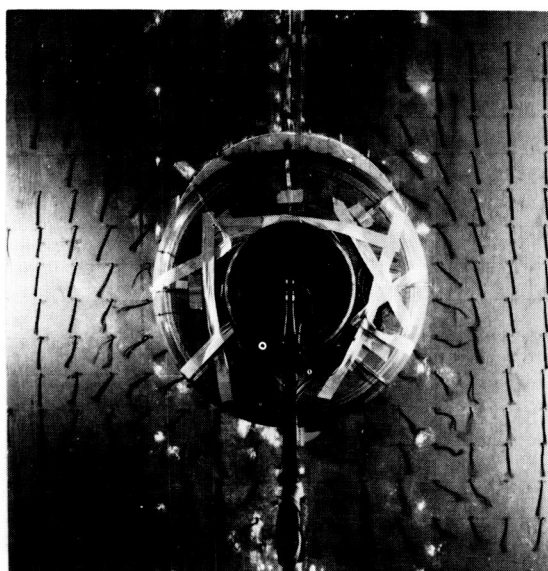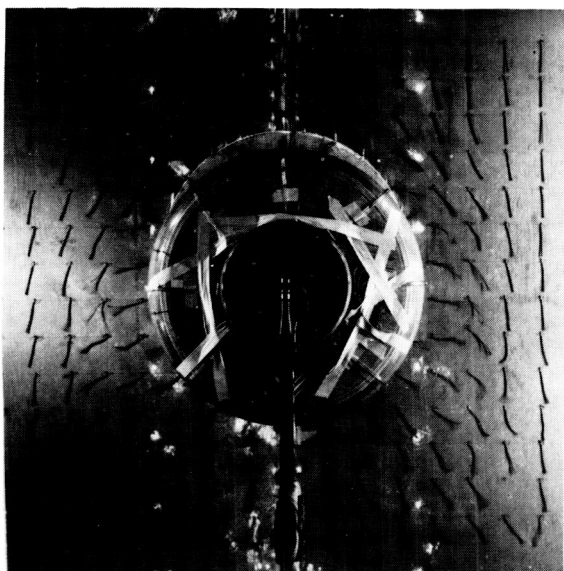
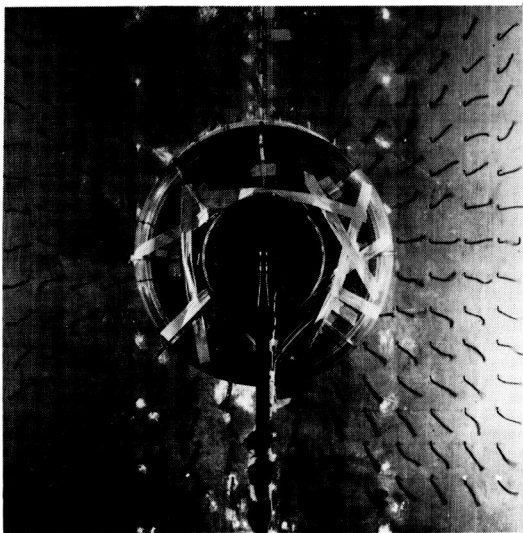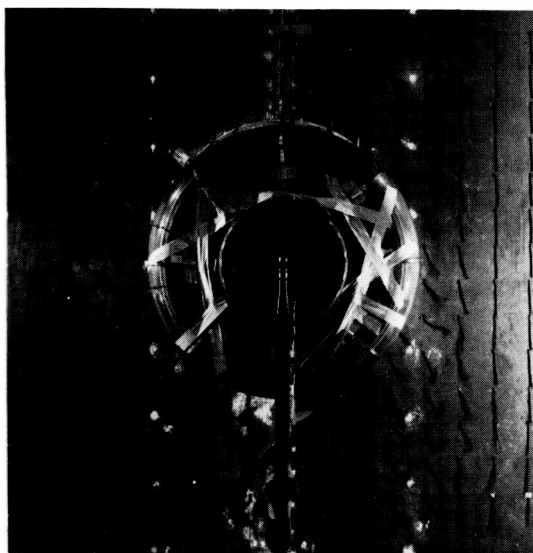$$\frac{V_\infty}{V_j} = 1.34$$

$$\frac{V_\infty}{V_j} = 2.24$$

Figure 17.- Concluded.

L-63-27

$$\frac{V_\infty}{V_j} = 0 \qquad V_\infty \downarrow \qquad \frac{V_\infty}{V_j} = .20$$

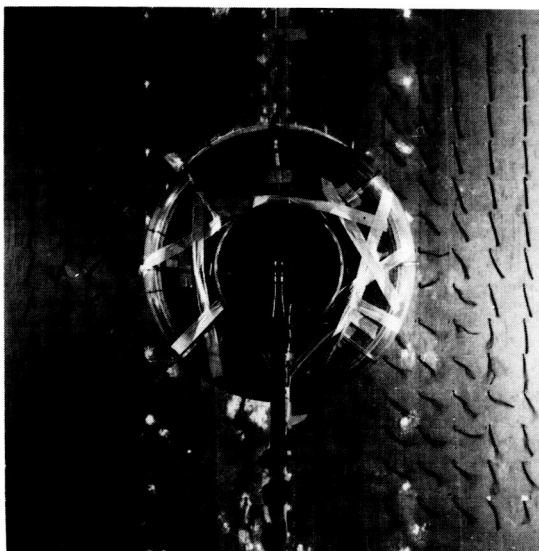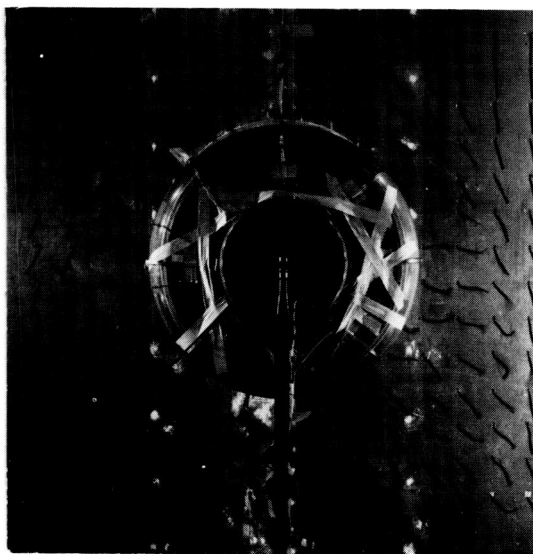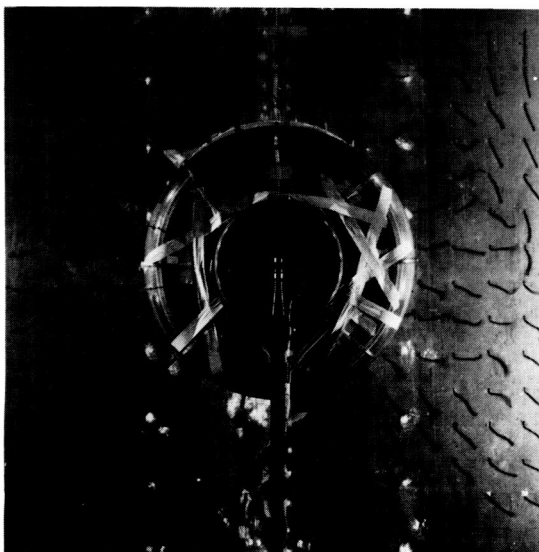$$\frac{V_\infty}{V_j} = .39 \qquad \frac{V_\infty}{V_j} = .48$$

L-63-28

Figure 18.- Photographs of tufts showing flow patterns at ground plane for various velocity ratios. $\alpha = 0°$; h/d = 0.10.

$$\frac{V_\infty}{V_j} = .59$$

V_∞

$$\frac{V_\infty}{V_j} = .94$$

$$\frac{V_\infty}{V_j} = 1.34$$

$$\frac{V_\infty}{V_j} = 2.08$$

Figure 18.- Concluded.

L-63-29